land

MDPI

Article

Reconstructing Floodplain Evolution from Sedimentary and Geochemical Records: Oxbow Lake–Natural Levee Systems Along the Upper Tisza River

György Szabó [1], Azin Rooien [1], Péter Czomba [2], Dávid Balázs [1], Tamás Mester [1], David Nicolás Matamoros Ojeda [1], Zoltán Túri [3], Gábor Négyesi [3] and Róbert Vass [1,*]

[1] Department of Landscape Protection and Environmental Geography, Institute of Earth Sciences, Faculty of Science and Technology, University of Debrecen, 4032 Debrecen, Hungary; szabo.gyorgy@science.unideb.hu (G.S.); azin.rooein@gmail.com (A.R.); balazs.david@science.unideb.hu (D.B.); mester.tamas@science.unideb.hu (T.M.); nicolas.matamoros@science.unideb.hu (D.N.M.O.)

[2] Institute of Environmental and Natural Sciences, University of Nyíregyháza, 4400 Nyíregyháza, Hungary; czomba.peter@nye.hu

[3] Department of Physical Geography and Geoinformatics, Institute of Earth Sciences, Faculty of Science and Technology, University of Debrecen, 4032 Debrecen, Hungary; turi.zoltan@science.unideb.hu (Z.T.); negyesi.gabor@scinece.unideb.hu (G.N.)

* Correspondence: vass.robert@science.unideb.hu

Abstract

Floodplain oxbow lakes and natural levees preserve sedimentary archives that can provide information on long-term changes in depositional environments. This study investigates three oxbow lake–natural levee pairs of different ages along the Upper Tisza River using 258 sediment records. Grain size composition, pH, electrical conductivity, $CaCO_3$-equivalent values, and organic carbon were characterized. Spearman correlation analysis was used to examine relationships among the measured properties, while principal component analysis (PCA) was performed using pH, electrical conductivity, organic carbon, and isometric log-ratio-transformed grain-size data. The profiles showed pronounced vertical and between-site heterogeneity, indicating that geomorphological position alone does not determine sediment properties. PCA identified four major sedimentological and geochemical gradients, whereas cluster analysis distinguished four broad sediment groups with distinct sedimentological and geochemical characteristics. These multivariate statistical analyses revealed relative vertical zonation and sedimentological and geochemical changes associated with oxbow-lake infilling and natural-levee development. Long-term mean sediment accumulation rates were estimated separately from the multivariate analyses using sediment thickness, documented channel-cutoff ages, and, where applicable, stratigraphic correlations. Time-averaged post-cutoff oxbow-lake sediment accumulation rates were approximately 10.2 cm yr^{-1} for GYM1, 4.56 cm yr^{-1} for GYM2, and $\leq$4.62 cm yr^{-1} for GYM3. For the natural levees, no accumulation rate was estimated for GYF1 because of the absence of an independent chronological marker, whereas tentative correlation of buried paleosol horizons in GYF2 and GYF3 with dated paleosols on the Bereg Plain suggests conditional long-term mean accretion rates of approximately 0.042–0.090 cm yr^{-1} for GYF2 and 0.032–0.069 cm yr^{-1} for GYF3, respectively. Integrating vertical sedimentological and geochemical records with multivariate statistical analyses and independent chronological and stratigraphic constraints therefore provides a framework for reconstructing relative depositional succession and estimating long-term sediment accumulation during floodplain evolution.

Check for updates

Academic Editor: Nick B. Comerford

Received: 3 September 2026
Revised: 5 October 2026
Accepted: 7 October 2026
Published: 9 October 2026

Copyright: © 2026 by the authors. Licensee MDPI, Basel, Switzerland. This article is an open access article distributed under the terms and conditions of the Creative Commons Attribution (CC BY) license.

Keywords: floodplain evolution; oxbow lake; natural levee; sedimentary archives; grain size composition; geochemical properties; principal component analysis; cluster analysis

1. Introduction

The most active areas of floodplains are the relatively flat alluvial surfaces adjacent to watercourses that are regularly inundated during floods [1,2]. The width of this zone depends on the hydrological characteristics of the watercourse and the local topographic conditions, as higher discharges and wider floodplains generally result in greater lateral inundation extent [3–5]. In many river systems, the natural lateral extent of floodplains has been substantially reduced by flood embankments. Such embankments have considerably diminished floodplain extent along numerous large rivers and altered the hydrological connectivity between rivers and their floodplains. Along the Rhine, embankment construction reduced the floodplain area from approximately 1400 km^2 to 950 km^2 [6]. Studies of the Lower Mississippi and Rhine demonstrated that flood embankments substantially altered floodwater and sediment transport, as well as geomorphological development within the floodplain [7,8]. Scheel et al. [9] further demonstrated the effects of embankments on floodplain connectivity at a larger spatial scale in the Wabash River basin. By restricting the lateral spreading of floodwaters, floodplain confinement concentrates overbank sediment deposition within the embanked floodplain, making oxbow lakes and natural levees key geomorphological archives of vertical sediment accretion and long-term floodplain evolution.

A similar situation has been observed within the Tisza River basin. According to the synthesis by Kiss [10], approximately 24,750 km^2 of the originally ~25,800 km^2 floodplain is currently protected by embankments, leaving only about 1050 km^2 as freely inundatable floodplain. Within the substantially confined floodplain, geomorphological processes that previously operated across broader areas, such as lateral channel migration and erosion, have been substantially reduced, with vertical accretion becoming increasingly dominant.

It is important to emphasize that inundation frequency varies considerably among different geomorphological units of floodplains, being primarily controlled by relative surface elevation and hydrological connectivity with the active channel [11,12].

The development of broad, relatively low-energy alluvial floodplains is characterized by considerable spatial and temporal variability, primarily related to the hydrological characteristics of flood inundation, floodplain topography, and sediment transport between the channel and floodplain [13–15]. Sedimentation processes can be particularly intensive in natural levees close to the channel and in lateral accretion features formed along the inner banks of meander bends [16]. Klasz et al. [16], studying the Danube floodplain east of Vienna, identified an average sediment accretion rate of approximately 11 mm/year in natural levee areas, compared with only 0.3 mm/year farther from the river over the past 120 years. Piégay et al. [17], examining 14 cutoff channels along the Ain River with ages ranging from 23 to 90 years, reported sedimentation rates of 0.11–2.4 cm/year, with a mean value of 0.65 cm/year. In a detailed comparison, the mean aggradation rate specifically within the cutoff channels was 1.03 cm/year, compared with 0.74 cm/year in the adjacent floodplain areas. The higher sedimentation rate was attributed to the more frequent inundation of cutoff channels. Siltation within cutoff channels also varies considerably through time. In recently abandoned channels of the Odra River in the Czech Republic, Sedláček et al. [18] measured initial aggradation rates of up to 32 cm/year, with this intensive initial phase lasting only 4–7 years. Kiss et al. [19] reported mean sedimentation rates of 1.3–2.4 cm/year in three cutoff channels along the Lower Maros

River. Aggradation was most intensive following nineteenth-century river regulation (1.9–2.4 cm/year), subsequently declining to 1.4–2.1 cm/year between 1884/89 and the 1960s, and to 0.5–0.9 cm/year thereafter. Siltation within cutoff channels is generally a multiphase and nonlinear process. Toonen et al. [20] divided the development of abandoned channels into an initial phase controlled by a still-active proximal fluvial connection and a later phase characterized by complete channel abandonment and finer-grained distal sediment deposition. According to Constantine et al. [21], the geometry of the cutoff itself can influence how rapidly hydrological connectivity with the river is lost, while Toonen [20] demonstrated that, owing to changing hydrological connectivity, the same grain-size proxy may behave differently during different stages of aggradation.

Several methods can be applied to determine the extent and conditions of sediment deposition. The vertical and horizontal distribution of sediment grain size provides important information on sedimentation conditions and floodplain energy regimes [15]. For example, Walling et al. [15] found that sand fractions dominated the coastal zone of the River Ouse at distances of 20–40 m from the channel, whereas finer fractions prevailed farther from the river. Grain size changes can therefore be used to reconstruct spatial variations in floodplain sedimentation. Sedimentological marker layers of known age provide a relatively simple method for estimating sedimentation rates, particularly where river regulation, channel relocation, or changes in land use have produced distinctive sediment layers [10,19].

Floodplain sediment pH is important because it affects chemical weathering, mineral transformation, and organic matter decomposition, thereby influencing sediment stability and preservation [22]. Besides local geological conditions, pH is strongly influenced by organic matter mineralization and redox conditions within the sediment profile [14].

Electrical conductivity (EC) provides an integrated indicator of dissolved ionic constituents and may therefore reflect changes in the hydrochemical conditions of floodplain sediments. Variations in EC can be influenced by hydrological processes such as inundation, infiltration, evaporation, and groundwater–surface water interactions, which control the dilution, transport, and retention of dissolved salts [23,24].

Calcium carbonate ($CaCO_3$) content is relevant because it influences sediment pH and consequently affects weathering, mineral transformation, and the preservation of organic matter within sediment sequences.

Organic carbon (OC) content and its spatial distribution contribute significantly to reconstructing floodplain surface development. Studies of floodplain sediments, such as those in the Rocky and Cascade Mountains, demonstrate that while OC concentrations are often elevated near the sediment surface due to modern vegetation inputs and pedogenesis, vertical profiles show substantial complexity rather than a simple downward decline [25]. Vertical OC profiles may show substantial variability with depth, including subsurface enrichment associated with differences in geomorphic setting and sedimentary conditions [25]. Furthermore, OC accumulation is influenced by geomorphic position and floodplain surface characteristics, which affect vegetation development, sedimentation, and organic-matter preservation [25].

For longer-term reconstruction, vertical sediment profiles can be analyzed using marker layers, including known flood deposits, anthropogenic pollutants, and radioactive isotopes. The ^{137}Cs isotope binds strongly to fine-grained soil particles and is therefore widely used to estimate sediment accretion or erosion over several decades [26,27]. Heavy metal marker layers can likewise be used to identify sedimentation associated with historically dated pollution events, such as the 2000 heavy-metal contamination of the Tisza River [28,29]. Pollen analysis can contribute to reconstructing temporal changes in sedimentation by identifying stratigraphic pollen assemblages and the palaeoenvironments they

represent [30]. Comparison of sediment thickness with the corresponding time intervals allows the rate and temporal dynamics of floodplain accretion to be quantified.

Floodplain depositional dynamics can be reconstructed using several complementary dating methods. Radiocarbon (^{14}C) dating of organic-rich layers enables long-term accretion rates to be estimated [31]. Optically Stimulated Luminescence (OSL) directly estimates the depositional age of sediment and can therefore be used to determine sedimentation rates of individual layers and temporal changes in depositional dynamics [32–34].

The present study extends our previous investigation of the Gyüre floodplain [35] both in the temporal–spatial coverage of the sedimentary record and in its methodological and interpretative framework. Whereas the previous study focused on two oxbow lake–natural levee pairs and predominantly on their upper sediment sequences, the present dataset includes an additional, younger oxbow lake–natural levee pair and substantially deeper sediment sequences, thereby covering three generations of floodplain landforms. Of the 258 analytical records used in the present study, 45 (17.4%) were obtained by aggregating previously reported 2-cm measurements from the upper sections of four profiles to the uniform 10-cm resolution applied here; the remaining 213 records (82.6%) represent sediment sections not included in [35]. The multivariate analysis was also refined by treating grain-size fractions as compositional data and applying an isometric log-ratio (ILR) transformation prior to PCA. Most importantly, the extended vertical records allow the statistical sediment groups to be interpreted in their stratigraphic context and related to changes in depositional and post-depositional conditions rather than merely to differences among geomorphological settings. This provides a basis for reconstructing and comparing the longer-term aggradation of oxbow lakes and accretion of natural levees across different stages of floodplain evolution. Rooien et al. [36], using ^{137}Cs as a chronological tracer in the same GYM2 oxbow lake, estimated a mean sediment accumulation rate of approximately 0.6 cm yr^{-1} for the upper part of the infill since the mid-1960s. This comparatively low recent rate indicates that sediment accumulation in the cutoff channel may have slowed substantially during the later stages of infilling.

Despite these advances, comparatively few studies have integrated multi-metre sedimentary records from oxbow lake–natural levee systems of different developmental stages with a multivariate analytical framework that explicitly accounts for the compositional nature of grain-size data, while also incorporating available historical and stratigraphic chronological constraints. The close spatial proximity of the three oxbow lake–natural levee pairs, combined with their different developmental stages, provides a comparative framework for examining how sedimentary and geochemical characteristics vary through successive stages of floodplain evolution under broadly similar fluvial and geological conditions.

Our research addresses the following questions:

RQ1. What sedimentological and geochemical differences characterize the vertical sediment sequences of oxbow lakes of different ages and their associated natural levees?

RQ2. What sedimentological and geochemical patterns and statistically distinct sediment groups can be identified that reflect different floodplain environments and depositional processes?

RQ3. How can multivariate statistical analyses reveal sedimentological and geochemical changes during oxbow-lake infilling and natural-levee development, and how do these changes reflect successive floodplain depositional environments?

RQ4. What long-term mean sediment accumulation rates can be estimated for the investigated oxbow lakes and natural levees based on their vertical sedimentary sequences and grain-size changes, together with available historical chronological information and regional stratigraphic correlations?

2. Materials and Methods

2.1. Study Area and Geomorphological Setting

The Tisza River, originating in the Northeastern Carpathians, is the second largest river in Hungary, with a drainage basin covering 157,186 km^2. Upon reaching the Hungarian Great Plain, it develops a meandering planform and deposits a substantial proportion of the gravelly sediment load characteristic of its piedmont section [37,38].

The study area is located in northeastern Hungary, within the floodplain of the Upper Tisza River, between the settlements of Gyüre and Tiszaszalka, at river kilometres 674–677 (Figure 1). The area forms part of the eastern margin of the alluvial floodplain of the Bereg Plain. In the wider surroundings of the investigated reach, approximately two dozen overdeveloped meander bends were cut off during river regulation works initiated in the mid-19th century.

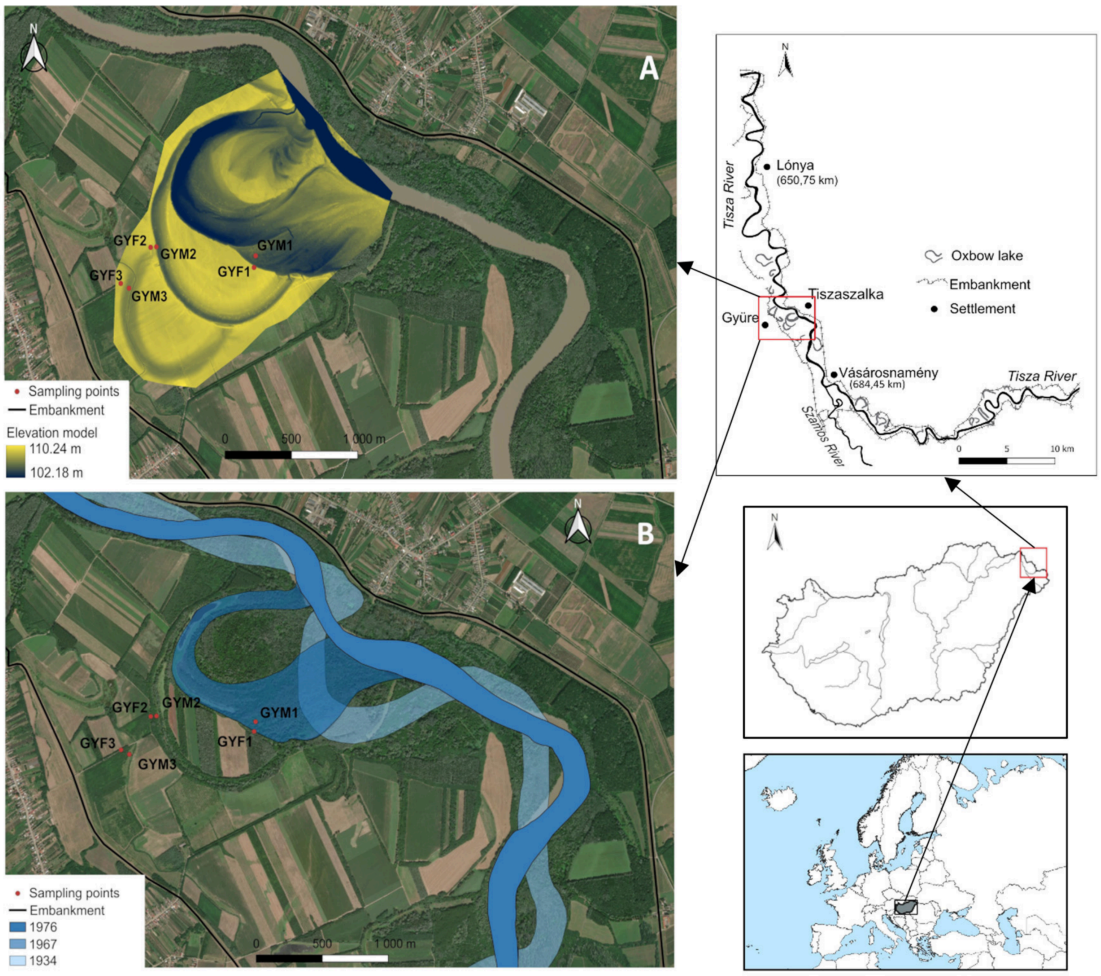


Figure 1. Location of the Gyüre active floodplain study area and the sampling sites. (**A**): Elevation of the study area. (**B**): Changes in the planform of the Tisza River.

As a consequence of river regulation, the channel length between the gauging stations located at the upstream and downstream limits of the study area, at Vásárosnamény (684.45 km) and Lónya (650.75 km), respectively, was reduced by approximately 40%, from 55.8 km to 33.7 km, while the channel gradient increased from 4.4 cm/km to 7.3 cm/km [39]. In parallel with channel regulation, the active floodplain was also established and, along the investigated reach, is typically bounded by flood embankments located 400–3500 m apart. In several locations, the embankments also enclose former meander bends that were cut off during river regulation.

Due to the geographical position of the drainage basin, significant floods may occur during as many as three periods within a single year [40]. In March–April, floods generated by snowmelt may propagate downstream during spring. In early summer, flooding may develop in response to frontal systems arriving from the Atlantic Ocean, whereas autumn cyclonic activity originating in the Mediterranean region frequently generates floods in November–December [41].

The gauging station at Tivadar, located approximately 30 km upstream of the study area (705.7 rkm; 105.4 m asl), provides daily water-level records for the period 1901–2013. These data indicate a long-term increasing trend in annual maximum water levels [42]. Partial inundation of the active floodplain associated with an elevation of 109 m asl occurred in 98 of the 113 years examined, with inundation lasting an average of 9 days per year. Complete inundation of the active floodplain, reaching an elevation of 110.2 m asl, occurred in 54 years, with an average annual inundation duration of 4 days.

At Vásárosnamény, the mean discharge of the river is 352 m^3/s, while the recorded minimum and maximum discharges are 43 m^3/s and 3702 m^3/s, respectively. The annual volume of suspended sediment transported by the river at this cross-section is approximately 0.9 million m^3. Based on bed-material samples collected from four cross-sections along an approximately 6-km-long river reach encompassing the study area, the mean grain diameter was 0.52 mm [38].

The width of the active floodplain along the Upper Tisza generally ranges between 500 and 3500 m, whereas values of 1600–3000 m were measured within the study area. The relatively large width of the active floodplain is primarily attributable to the presence of three generations of oxbow lakes of different ages located in close proximity to one another (Figure 1).

The study area was selected using Google Earth. Subsequently, a LiDAR-based digital elevation model acquired in 2022 by Envirosense Hungary Ltd. (Debrecen, Hungary) was used for the precise identification and delineation of the geomorphological forms. The DEM was provided as a raster with a spatial resolution of 1 × 1 m (1 m^2 per pixel). Information on the vertical accuracy of the DEM was not available. The data were visualized and analyzed using Global Mapper v27 and QGIS software v4.2.3 (Figure 2).

The three oxbow lake–natural levee pairs were selected because they occur within a relatively small section of the same active floodplain but represent three different generations of floodplain development. The oxbow lakes were designated GYM1, GYM2, and GYM3, and their associated natural levees GYF1, GYF2, and GYF3, respectively (Figure 1). This spatial arrangement provides an opportunity to compare sedimentary records of different developmental stages while minimizing differences in the broader fluvial and geological setting. Within each pair, sampling locations were selected to represent the characteristic sedimentary environment of the respective geomorphological form and to maintain close spatial correspondence between the oxbow lake and its associated natural levee. For all three natural levee profiles, sites affected by regular ploughing were deliberately avoided in order to minimize anthropogenic disturbance of the upper sediment sequence. Within the oxbow lakes, profiles were positioned away from the immediate channel margins to reduce the potential influence of bank erosion and local sediment reworking. These criteria were intended to maximize the comparability of the three oxbow lake–natural levee systems and the preservation of their vertical sedimentary records. Additional details on the geomorphological setting and the previously investigated sampling sites are provided in our earlier study [35].

The exact date of cutoff of the oldest oxbow, GYM3, cannot be determined; however, the process must have occurred before 1785, as the First Military Survey already depicted the channel as inactive. Subsequent erosional and aggradation processes have modified the

former channel, which currently extends for approximately 1.5 km and is 130–140 m wide. Persistent water cover is absent, and the former channel bank is difficult to identify due to subsequent erosion. The elevation of the sampling site is 106.1 m asl. An artificial drainage channel, approximately 1.5 m wide and 1 m deep, runs along the thalweg of the former channel. The associated GYF3 natural levee crest is approximately 1.5–2.5 m higher than the deepest part of the channel, with the sampling site located at an elevation of 108.6 m asl. Field observations clearly indicate substantial siltation within the former channel.

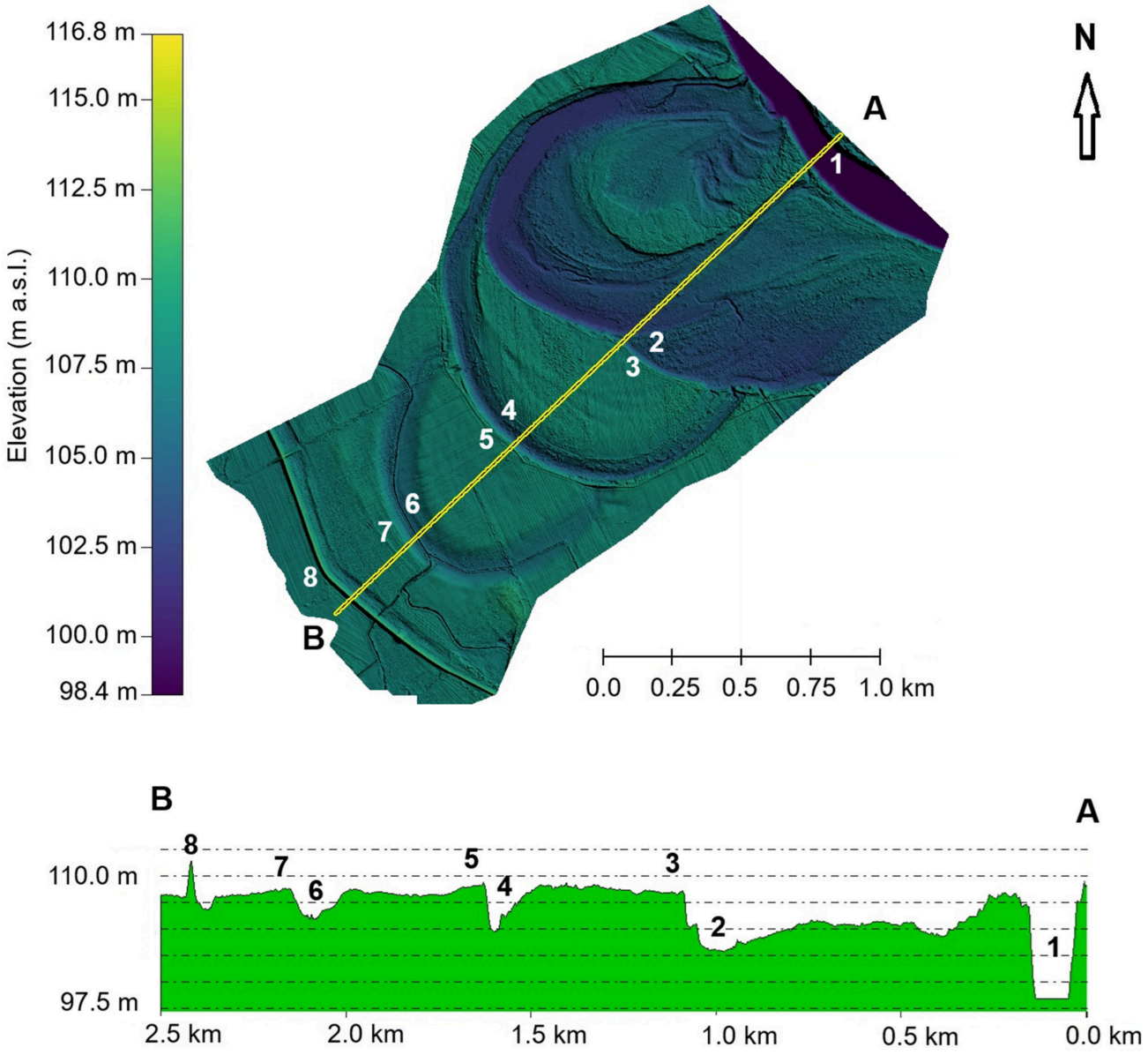


Figure 2. Elevation data of the study area presented along a cross-section (A-B). 1: Tisza River, 2: GYM1 oxbow (cut off 1974), 3: GYF1 natural levee, 4: GYM2 oxbow (cut off 1852), 5: GYF2 natural levee, 6: GYM3 oxbow (cut off earlier than 1785), 7: GYF3 natural levee, 8: flood embankment.

The younger oxbow lake, GYM2, was created during the river regulation works carried out in 1852. Its present-day length is 2.17 km, although a section of the younger channel has been destroyed by subsequent lateral erosion of the Tisza. The channel is 90–110 m wide, and, similarly to GYM3, no permanent water cover has developed. The sampling site is located at 104.4 m asl. The bank face of the GYM2 oxbow lake is relatively steep, with an

elevation difference of 3.5–5 m between the natural levee and the former channel bed. The sampling site on the GYF2 natural levee is located at 109.3 m asl.

The youngest geomorphological feature is the GYM1 meander, which was cut off in 1974, together with the associated GYF1 natural levee. The meander was artificially cut off because lateral erosion by the river posed a threat to several settlements. During the 40 years preceding its cutoff, the meander migrated 1250 m downstream. As a consequence, the channel had not developed a sufficiently incised morphology and was characterized by numerous channel bars, while its width reached 500–550 m (Figure 1). The concave bank of the GYM1 cutoff channel is steeper than that of the older cutoff channel, and the elevation difference between the natural levee and the former channel bed is 4.5–6 m. The sampling site established on the natural levee is located at 108.70 m asl, whereas the sampling site within the cutoff channel is situated at 104.37 m asl.

2.2. Sampling and Laboratory Measurements

Sampling was conducted between 2023 and 2026 (Table 1). A total of six sampling profiles were established, with efforts made to select undisturbed locations. In the upper sections of the profiles, samples weighing approximately 1000 g were collected from the profile walls at 2 cm depth intervals. The previous study [35] was based on samples collected during the autumn 2023 field campaigns and included the upper sections of GYF2 (0–100 cm), GYF3 (0–100 cm), GYM2 (0–130 cm), and GYM3 (0–120 cm), analyzed at 2-cm resolution. For the present study, these measurements were averaged into 10-cm intervals to match the vertical resolution of the deeper auger samples and to provide a uniform resolution for the subsequent statistical analyses. Because bulk density was not determined for the individual 2-cm intervals, density-weighted averaging was not possible; arithmetic means were therefore used for the aggregation. For grain-size data, arithmetic averaging was performed on the original percentage fractions, and the ILR transformation was applied subsequently to the resulting 10-cm dataset used for PCA. These previously investigated sections account for 45 of the 258 analytical records (17.4%) in the present dataset, while the remaining 213 records (82.6%) originate from sediment sections not included in [35]. Sampling of the deeper layers was performed using an Eijkelkamp-type hand auger, reaching depths of 500 cm in GYF1, 500 cm in GYF2, 300 cm in GYF3, 550 cm in GYM1, 240 cm in GYM2, and 490 cm in GYM3. Samples weighing 250–500 g were collected at 10 cm depth intervals. For the GYM1 and GYF1 sections, sampling took place between the summer of 2025 and the summer of 2026.

Table 1. Site characteristics and parameters used for estimating sediment accumulation rates in the investigated profiles.

Profile	WGS 84 Coordinate	Profile/Pit Depth (cm)	Depth of Former Channel-Bed (cm)	Sampling Date
GYM1	N48° 10′ 32.44″; E22° 17′ 50.79″	0–550/0–120	530	2026
GYF1	N48° 10′ 31.23″; E22° 17′ 50.13″	0–500/0–100	–	2025
GYM2	N48° 10′ 38.76″; E22° 17′ 15.41″	0–240/0–130	780	2023
GYF2	N48° 10′ 38.45″; E22° 17′ 13.75″	0–500/0–100	–	2023
GYM3	N48° 10′ 28.69″; E22° 17′ 05.70″	0–490/0–120	1100	2023
GYF3	N48° 10′ 29.57″; E22° 17′ 03.45″	0–300/0–100	–	2023

In the oxbow lakes, we aimed to reach the sand-rich layer deposited within the still-active channel immediately prior to channel abandonment. This layer was interpreted as representing the sediment deposited during the final stage of active channel development.

Once the groundwater table was reached, a fully closed auger head was used to prevent mixing of the samples.

To determine the depth of the former channel bed in GYM2 and GYM3, drilling was continued beyond the systematically sampled sediment sequences using the motorized auger in autumn 2023. The sand-rich layer indicating the former active channel bed was reached at depths of 780 cm in GYM2 and 1100 cm in GYM3. Because the motorized auger did not allow systematic sampling at 10 cm intervals, these deeper sections were used only to identify the depth of the former channel bed and were not included in the sedimentological, geochemical, or statistical analyses. Accordingly, the analyzed sediment sequences extend to 240 cm in GYM2 and 490 cm in GYM3.

Sedimentological and geochemical analyses of the samples were conducted in the laboratory of the Institute of Earth Sciences, University of Debrecen. The analytical procedures applied here were consistent with those used in our previous study of the same floodplain [35].

Following drying at 40 °C, the sediment samples were homogenized and pulverized. For grain size analysis, particles larger than 0.2 mm were separated by sieving, whereas the grain size distribution of the fraction smaller than 0.2 mm was determined using the Köhn pipette method according to the MSZ-08-0205-1978 standard [43]. For the sedimentation analysis, a 10 g subsample was weighed to an accuracy of four decimal places. Aggregated particles were disaggregated by gentle rubbing with a rubber stopper in distilled water, and the resulting suspension was quantitatively transferred into a graduated cylinder. To prevent re-aggregation of the particles, 10 mL of sodium oxalate was added to the distilled-water suspension as a dispersing agent.

Grain size classification was performed according to the Mihăltz classification system. The following fractions were distinguished: coarse and medium-grained sand (2–0.2 mm), small-grained sand (0.2–0.1 mm), fine-grained sand (0.1–0.05 mm), coarse silt (0.05–0.02 mm), fine silt (0.02–0.002 mm), and clay (<0.002 mm) [44].

The pH was determined electrometrically in distilled water and 1 M potassium chloride (KCl) suspensions at a soil-to-solution ratio of 1:2.5. The suspensions were allowed to stand for 12 h before measurement, and pH was measured using a WTW pH 340 instrument according to the MSZ-08-0206/2-1978 standard [45]. The qualitative interpretation of soil reaction (strongly acidic, acidic, slightly acidic, neutral, slightly alkaline, alkaline, and strongly alkaline) was based on the pH classes associated with this standard. Acid-induced gas evolution was determined using a Scheibler calcimeter and expressed as $CaCO_3$ equivalent ($CaCO_3$ eq., %) in accordance with MSZ-08-0206/2-1978 [45]. Because the method is based on volumetric gas evolution following acidification, the resulting values are treated here as an operational calcimetric parameter rather than as a mineral-specific determination of calcite. Organic carbon (OC) content was determined using the Tyurin method, in accordance with the MSZ-08-0206/2-1978 [45] and MSZ-08-0210-1977 [46] standards, respectively.

Soil electrical conductivity (EC) was determined according to the MSZ 21470–2:1981 [47] standard. Electrical conductivity was measured in a 1:10 soil-to-water extract prepared using distilled water [47]. The data obtained from the individual analyses were organized in MS Excel, while statistical analyses were performed using the IBM SPSS 22 software package [48].

To eliminate differences arising from the different sampling depth resolutions and to ensure a consistent vertical resolution of the dataset, mean values were calculated at 10 cm depth intervals from the samples collected at 2 cm intervals within the upper 100–130 cm. This procedure resulted in a database with a uniform 10 cm vertical resolution, consistent with the data obtained from the deeper sediment sequences, which had already

been sampled at 10 cm intervals. The resulting standardized dataset was used for the statistical analyses.

2.3. Methods of Statistical Analysis

Before the statistical analyses, the distributional properties of the individual variables were examined. Normality was assessed using the Kolmogorov–Smirnov and Shapiro–Wilk tests, supplemented by visual evaluation of Q–Q plots. Since formal normality tests can be sensitive to even minor deviations from a normal distribution in larger samples, the distributions were evaluated by considering the test results and graphical assessment jointly. The results of the distributional analysis were also taken into account when selecting the correlation procedure used to examine relationships among the variables. Because the distributions of several variables deviated substantially from normality, the non-parametric Spearman rank correlation coefficient (ρ) was used to assess the strength and direction of monotonic relationships between variables. Statistical significance was defined at $p < 0.05$.

Principal component analysis (PCA) was applied to explore multivariate relationships among the physical and chemical properties of the investigated sediment samples and to reduce the dimensionality of the dataset. The aim of the analysis was to condense the information contained in correlated sedimentological and geochemical variables into a smaller number of mutually independent principal components, thereby identifying the main gradients controlling variability among the sediment samples.

In the PCA, pH(H_2O), pH(KCl), electrical conductivity (EC), organic carbon (OC), and the grain-size data were considered. The Scheibler-derived $CaCO_3$-equivalent variable was excluded from the PCA because, in low-pH and potentially sulfidic sediments, acidification may release gases other than CO_2, particularly H_2S, which may contribute to the measured gas volume. Consequently, the calcimetric values could not be interpreted unequivocally as carbonate content for all samples. However, the original percentage values of the grain-size fractions were not entered directly into the analysis. Grain-size data can be considered compositional data because the individual fractions jointly represent the complete sample and their sum equals 100% for each sample. Due to this constant-sum constraint, the individual fractions are not mathematically independent: an increase in the relative proportion of one fraction necessarily results in a decrease in the relative proportion of one or more other fractions. Consequently, correlation and principal component analyses performed on raw percentage values may produce artificial correlations and redundancy. During the preliminary analysis, this issue was also reflected in the non-positive-definite nature of the correlation matrix. Therefore, grain-size composition was treated as compositional data, and an isometric log-ratio transformation (ILR) was applied before PCA. The ILR transformation maps constant-sum compositions into orthonormal coordinates while preserving the relevant geometric properties of the simplex, thereby enabling the appropriate application of conventional multivariate statistical methods to compositional data [49].

Six grain size fractions were determined in the analyses: 2–0.2 mm, 0.2–0.1 mm, 0.1–0.05 mm, 0.05–0.02 mm, 0.02–0.002 mm, and <0.002 mm. The coarsest fraction (2–0.2 mm) contained zero values in numerous samples. Because log-ratio transformation cannot be applied directly to zero values, and artificial replacement of zeros was deliberately avoided, this fraction was excluded from the ILR transformation. The remaining five fractions had positive values in all samples; therefore, no zero replacement was required for these components.

Four mutually orthogonal ILR coordinates were constructed from the five positive grain-size fractions using a sequential binary partition (SBP). The partition was designed to ensure that the individual coordinates represented sedimentologically interpretable grain size contrasts. Let x_1 denote the 0.2–0.1 mm sand fraction, x_2 the 0.1–0.05 mm fine-grained

sand fraction, x_3 the 0.05–0.02 mm coarse silt fraction, x_4 the 0.02–0.002 mm fine silt fraction, and x_5 the <0.002 mm clay fraction. The four ILR coordinates were calculated as follows (Equations (1)–(4)):

$$\mathrm{ILR}_1 = \sqrt{\frac{6}{5}} \ln\left(\frac{\sqrt{x_1 x_2}}{\sqrt[3]{x_3 x_4 x_5}}\right) \quad (1)$$

$$\mathrm{ILR}_2 = \sqrt{\frac{1}{2}} \ln\left(\frac{x_1}{x_2}\right) \quad (2)$$

$$\mathrm{ILR}_3 = \sqrt{\frac{2}{3}} \ln\left(\frac{\sqrt{x_3 x_4}}{x_5}\right) \quad (3)$$

$$\mathrm{ILR}_4 = \sqrt{\frac{1}{2}} \ln\left(\frac{x_3}{x_4}\right) \quad (4)$$

ILR_1 expresses the relative balance between the two sand fractions and the finer silt–clay fractions; ILR_2 represents the ratio between the two sand fractions; ILR_3 represents the ratio of the silt fractions to clay; while ILR_4 represents the relative ratio between coarse and fine silt. The ILR coordinates are not grain-size percentages but logarithmic contrasts. A positive value indicates the relative dominance of the fraction or group of fractions appearing in the numerator of the respective equation, whereas a negative value indicates the relative dominance of the component or group of components appearing in the denominator. Accordingly, an increase in ILR_1, for example, indicates an increase in the relative contribution of the sand fractions compared with the silt and clay fractions.

A total of eight variables were therefore included in the PCA: pH(H_2O), pH(KCl), EC, OC, and ILR_1, ILR_2, ILR_3, and ILR_4. The analysis was based on 258 sediment samples. Since the included variables differed in their units of measurement and numerical scales, PCA was performed on standardized variables using the correlation matrix. This ensured that variables with different magnitudes did not exert disproportionately different effects on the resulting components solely because of their measurement scale or variance.

The suitability of the variables for PCA was assessed using the Kaiser–Meyer–Olkin (KMO) measure of sampling adequacy and Bartlett's test of sphericity. The number of components was determined according to the Kaiser criterion, retaining components with eigenvalues greater than 1. The selection of the number of components was additionally evaluated by visual inspection of the scree plot. Based on these two criteria, four principal components were retained. To improve the interpretability of the component structure, orthogonal Varimax rotation with Kaiser normalization was applied. The rotated component matrix was used to determine which of the original and ILR-transformed variables showed the strongest associations with each principal component. Component scores for individual samples were calculated using the regression method and subsequently used to examine the position of the samples within multivariate space and to further investigate variability both within and among the individual sampling profiles.

Hierarchical cluster analysis was applied to classify the 258 sediment samples according to their physicochemical properties. A total of 10 original variables were included in the analysis: pH(H_2O), pH(KCl), EC, OC, and the six grain-size fractions. The Scheibler-derived $CaCO_3$-equivalent variable was excluded from the cluster analysis for the same methodological reason as in the PCA. To eliminate the effects of differences in measurement scales, all variables were Z-standardized. Clustering was performed using Ward's method with squared Euclidean distance. The original grain-size fractions were retained in the cluster analysis because the coarsest fraction, which contains numerous zero values and was therefore excluded from the ILR transformation, provides important sedimentological information on coarse channel-bed deposits.

The number of clusters was evaluated based on the dendrogram, changes in the agglomeration coefficients, cluster size, and sedimentological interpretability. Based on these criteria, the four-cluster solution was retained as the primary classification because it provided a parsimonious and sedimentologically interpretable grouping of the samples.

The clusters were characterized using the means and standard deviations of the original, non-standardized variables. The discriminatory contribution of individual variables among the clusters was assessed using the F-statistic from one-way ANOVA, with the results interpreted descriptively in view of the fact that the variables had also been used to construct the clusters. To assess the sensitivity of the four-cluster solution to the compositional nature of the grain-size data and to the strong correlation between the two pH variables, an additional hierarchical cluster analysis was performed using the four ILR coordinates together with pH(H_2O), EC, and OC. These seven variables were Z-standardized, and Ward's method with squared Euclidean distance was applied. The number of clusters was fixed at four to allow direct comparison with the primary classification.

3. Results

The descriptive statistics calculated for each profile revealed substantial differences in both sedimentological and geochemical properties (Table 2). Among the natural levee profiles, GYF1 was characterized by relatively high proportions of the sand fractions and a low clay content (11.8%), whereas the older GYF3 exhibited a finer-grained composition, with a mean fine silt content of 41.4% and a mean clay content of 25.4%. Substantial differences were also observed among the oxbow lake profiles. GYM1 was characterized by a higher mean pH (7.48) and EC (571.8), while GYM2 had the highest mean $CaCO_3$-equivalent value (6.40%). Across its complete analyzed 0–490 cm sequence, GYM3 exhibited a fine-grained composition (51.6% fine silt and 29.4% clay), a mean pH(H_2O) of 5.42, and the highest mean OC content (3.24%) among the investigated profiles; these values are strongly influenced by the distinctive organic-rich deeper interval between 200 and 490 cm. Based on the standard deviations, several parameters also exhibited considerable within-profile variability.

Table 2. Descriptive statistics (mean ± SD and median) of the sedimentological and geochemical parameters of the six investigated sediment profiles.

Parameter	GYF1 (0–500 cm) (*n* = 50)	GYF2 (0–500 cm) (*n* = 50)	GYF3 (0–300 cm) (*n* = 30)	GYM1 (0–550 cm) (*n* = 55)	GYM2 (0–240 cm) (*n* = 24)	GYM3 (0–490 cm) (*n* = 49)
pH(H_2O)	6.64 ± 0.34 Med. 6.79	6.69 ± 0.53 Med. 6.92	6.30 ± 0.41 Med. 6.42	7.48 ± 0.17 Med. 7.47	7.37 ± 0.75 Med. 7.70	5.42 ± 1.12 Med. 4.81
pH(KCl)	5.50 ± 0.36 Med. 5.39	5.47 ± 0.38 Med. 5.48	4.84 ± 0.45 Med. 5.04	7.05 ± 0.14 Med. 7.05	6.42 ± 0.90 Med. 6.87	4.37 ± 1.04 Med. 3.80
EC (µS cm^{-1})	111.6 ± 87.5 Med. 73.7	393.0 ± 370.4 Med. 367.0	238.3 ± 179.9 Med. 154.3	571.8 ± 254.8 Med. 500.0	273.2 ± 70.4 Med. 255.2	406.7 ± 176.6 Med. 425.0
$CaCO_3$ eq. (%)	3.98 ± 0.99 Med. 3.65	4.83 ± 0.83 Med. 4.62	4.47 ± 0.51 Med. 4.53	5.11 ± 0.70 Med. 5.11	6.40 ± 0.74 Med. 6.44	4.40 ± 0.67 Med. 4.17
OC (%)	1.08 ± 0.92 Med. 0.84	1.11 ± 0.87 Med. 0.85	1.44 ± 1.56 Med. 0.90	2.08 ± 0.94 Med. 2.11	1.59 ± 0.78 Med. 1.41	3.24 ± 1.65 Med. 2.72
Coarse and medium sand (2–0.2 mm) (%)	0.31 ± 0.55 Med. 0.10	0.01 ± 0.05 Med. 0.00	0.08 ± 0.11 Med. 0.00	2.17 ± 6.49 Med. 0.00	0.00 ± 0.00 Med. 0.00	0.03 ± 0.10 Med. 0.00
Small-grained sand (0.2–0.1 mm) (%)	17.27 ± 12.41 Med. 14.85	6.61 ± 5.07 Med. 5.05	7.50 ± 6.63 Med. 5.34	14.17 ± 14.57 Med. 7.10	3.47 ± 2.48 Med. 3.05	3.68 ± 3.22 Med. 2.90

Table 2. *Cont.*

Parameter	GYF1 (0–500 cm) (*n* = 50)	GYF2 (0–500 cm) (*n* = 50)	GYF3 (0–300 cm) (*n* = 30)	GYM1 (0–550 cm) (*n* = 55)	GYM2 (0–240 cm) (*n* = 24)	GYM3 (0–490 cm) (*n* = 49)
Fine-grained sand (0.1–0.05 mm) (%)	18.22 ± 7.31 Med. 19.35	11.57 ± 7.84 Med. 9.55	8.15 ± 3.34 Med. 7.48	13.58 ± 8.10 Med. 11.90	9.48 ± 11.00 Med. 4.57	3.24 ± 2.33 Med. 2.70
Coarse silt (0.05–0.02 mm) (%)	23.16 ± 5.79 Med. 22.75	19.78 ± 8.14 Med. 20.04	17.45 ± 5.60 Med. 16.29	19.32 ± 7.43 Med. 20.70	16.33 ± 9.81 Med. 14.65	12.10 ± 7.09 Med. 10.20
Fine silt (0.02–0.002 mm) (%)	29.21 ± 12.08 Med. 27.55	35.72 ± 9.12 Med. 34.15	41.43 ± 8.87 Med. 41.83	38.25 ± 15.57 Med. 42.48	47.94 ± 13.51 Med. 53.93	51.56 ± 4.53 Med. 51.94
Clay (<0.002 mm) (%)	11.83 ± 3.67 Med. 11.40	26.30 ± 14.13 Med. 25.35	25.39 ± 7.85 Med. 26.30	12.50 ± 6.74 Med. 12.70	22.77 ± 8.45 Med. 24.02	29.39 ± 8.62 Med. 29.40

Values are presented as mean ± standard deviation, Med. = median.

3.1. Vertical Variability of Sediment Properties Across the Studied Profiles

The grain size composition and its vertical variability differed substantially among the six investigated profiles (Figure 3). Finer fractions, particularly fine silt and clay, were dominant in most profiles; however, several profiles also contained clearly distinguishable, sand-enriched layers. The GYM1 profile exhibited particularly pronounced vertical changes. While the upper and middle sections were predominantly characterized by finer-grained sediments, the proportion of sand fractions gradually increased below approximately 400 cm, becoming dominant in the lowermost part of the profile. In contrast, GYM2 exhibited a relatively fine-grained composition, with fine silt and clay dominating a substantial part of the profile, whereas sandier sediments occurred primarily in the lower section. The GYM3 profile was likewise predominantly composed of fine-grained sediments; however, several smaller-scale changes in grain size composition were observed throughout the profile. Unlike GYM1, no increase in the proportion of sand fractions was observed in the deeper layers investigated down to 490 cm.

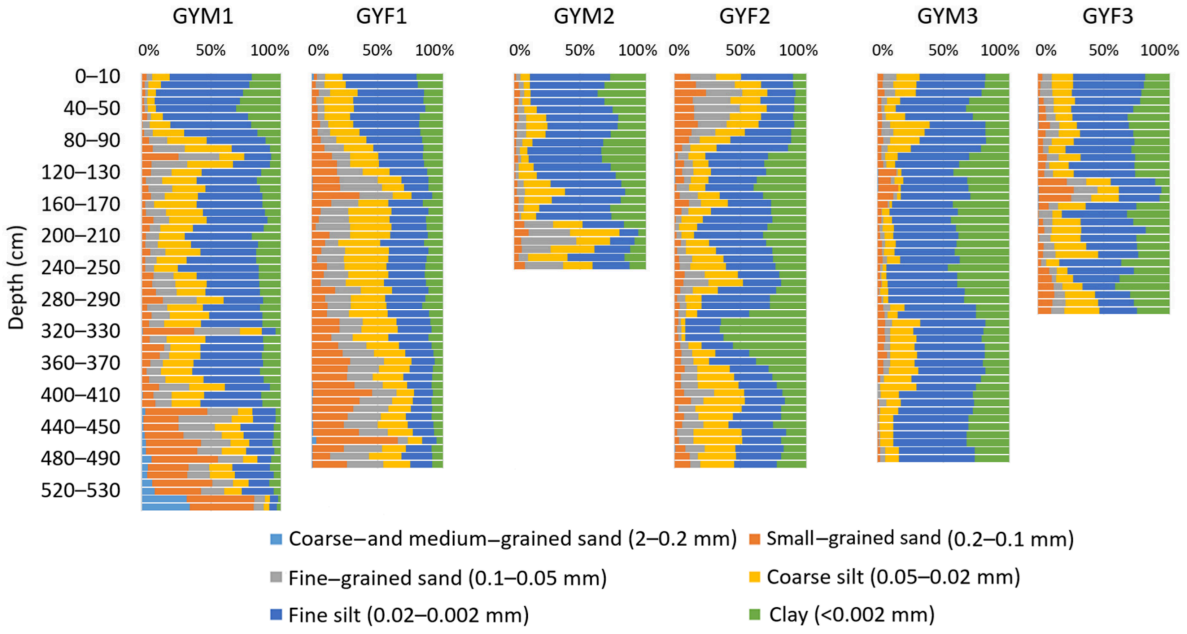


Figure 3. Vertical variation in grain-size composition of the oxbows (GYM1–GYM3) and natural levees (GYF1–GYF3) sediment profiles.

The natural levee profiles (GYF1–GYF3) generally exhibited greater vertical heterogeneity, reflected in alternating layers with sandier and finer-grained compositions. This

resulted in particularly pronounced changes in grain size composition in the GYF1 and GYF3 profiles. Overall, the grain size distributions differed not only between oxbow lake and natural levee sediments, but also substantially among the vertical sedimentary structures of profiles associated with the same geomorphological unit.

The sediment profiles covered a broad range of soil reaction classes, from acidic to slightly alkaline conditions, with considerable differences among profiles and with depth (Figure 4). In all profiles, pH(H_2O) values were consistently higher than the corresponding pH(KCl) values. GYM1 showed the most uniform vertical pattern, with only minor fluctuations throughout the profile. GYF1 and GYM2 displayed somewhat greater variability, but without a pronounced overall trend with depth. GYF2 was characterized by relatively high and stable pH values, particularly in the middle and lower parts of the profile. The most pronounced vertical change occurred in GYM3, where both pH(H_2O) and pH(KCl) decreased markedly below approximately 180–200 cm, reaching the lowest values among the studied profiles. GYF3 showed moderate vertical variability, with generally higher pH values than the deeper part of GYM3. Overall, the results indicate substantial profile-specific differences in both pH level and vertical variability.

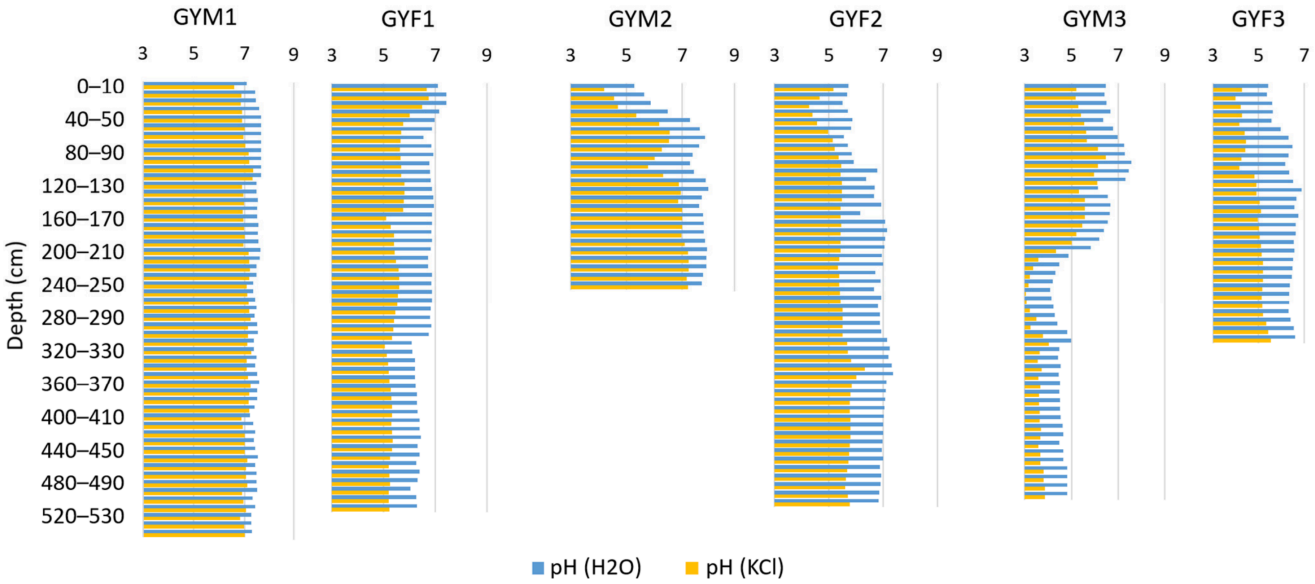


Figure 4. Vertical variation in pH(H_2O) and pH(KCl) of the oxbows (GYM1–GYM3) and natural levees (GYF1–GYF3) sediment profiles.

Electrical conductivity (EC) showed considerable differences both among the sediment profiles and with depth (Figure 5). Relatively low and vertically stable EC values characterized GYF1 and GYM2, while GYM1 exhibited a pronounced increase below approximately 200 cm, reaching its highest values at around 250–300 cm, followed by a gradual decrease towards the bottom of the profile. The most prominent anomalies occurred in GYF2, where exceptionally high EC values were recorded at approximately 110–120 and 150–160 cm, with the latter exceeding 2000 µS/cm. Below this interval, EC increased more gradually to a secondary maximum at around 320–340 cm before declining again. In GYM3, EC generally increased with depth to a maximum at approximately 310–330 cm and subsequently decreased, whereas GYF3 showed a marked increase in the lowermost part of the profile. Overall, EC displayed pronounced profile-specific vertical patterns, with the greatest variability observed in GYF2 and GYM1.

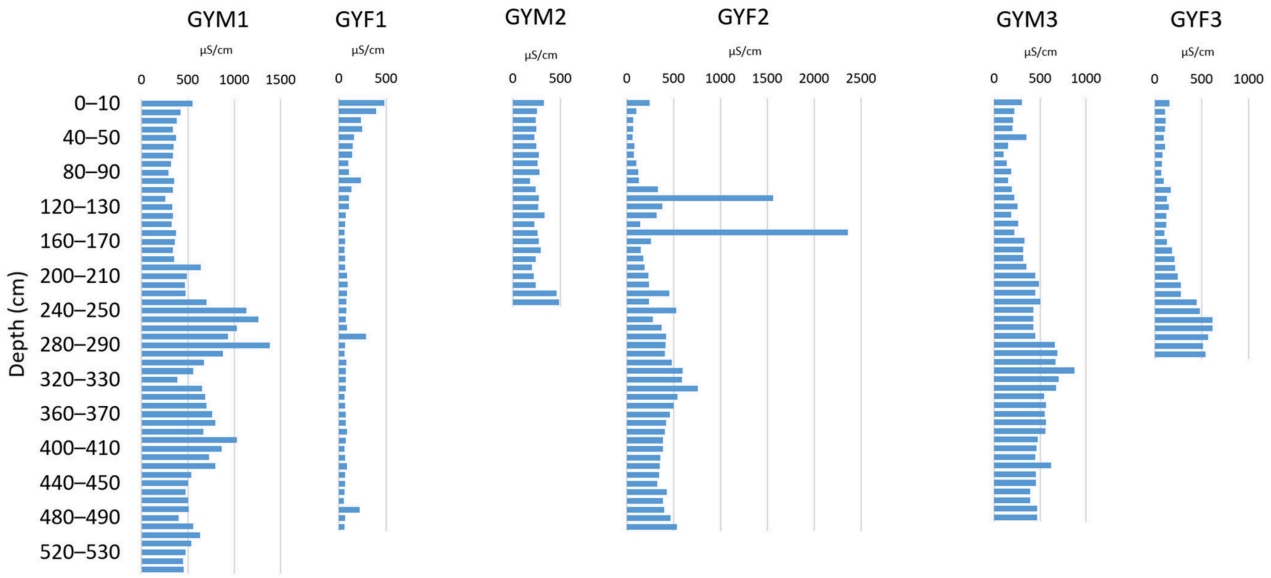


Figure 5. Vertical variation in electrical conductivity (EC) of the oxbows (GYM1–GYM3) and natural levees (GYF1–GYF3) sediment profiles.

The Scheibler-derived $CaCO_3$-equivalent values showed moderate differences among the six profiles, with most values ranging approximately between 3 and 7% (Figure 6). GYM2 was characterized by relatively high and vertically uniform $CaCO_3$-equivalent values, particularly in the upper part of the profile. In contrast, GYM1 displayed greater vertical variability, with generally higher values in the lower half and a pronounced maximum at approximately 430–440 cm. GYF1 showed a clear decrease from relatively high $CaCO_3$-equivalent values in the uppermost layers to lower values below approximately 100–120 cm, followed by only minor fluctuations at greater depths. GYF2 exhibited moderate vertical variation without a consistent depth-related trend, while GYM3 and GYF3 generally showed somewhat lower $CaCO_3$-equivalent values and relatively limited variability. Overall, the distribution of this operational calcimetric parameter was less vertically heterogeneous than EC, although distinct profile-specific patterns were evident.

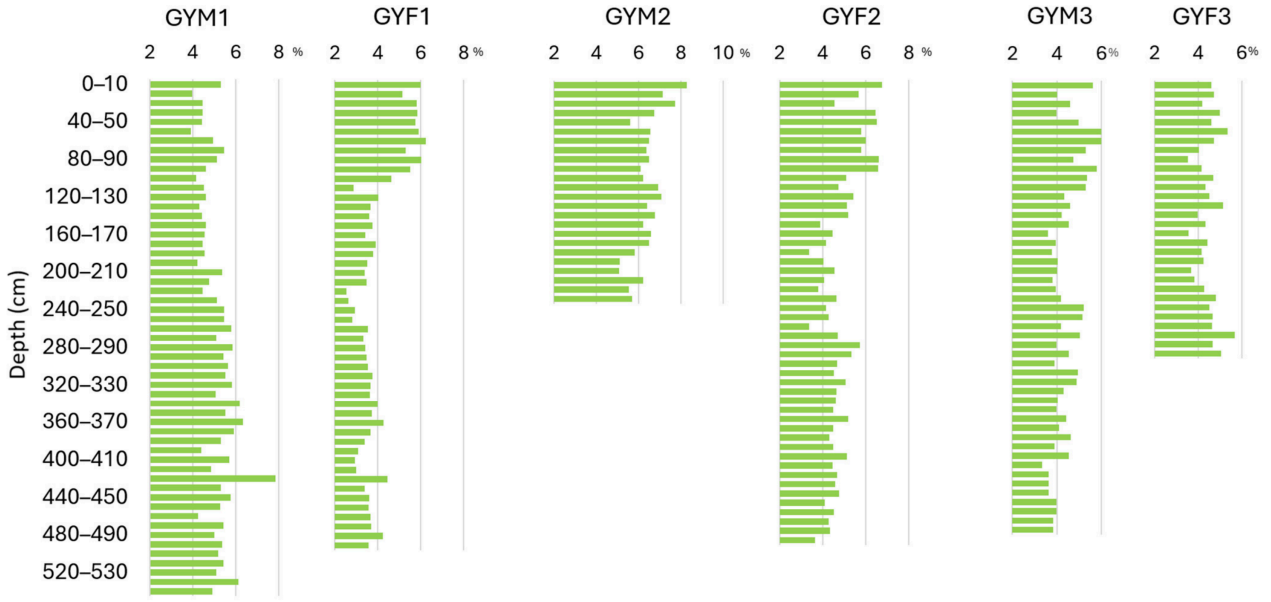


Figure 6. Vertical variation in $CaCO_3$-equivalent values of the oxbows (GYM1–GYM3) and natural levees (GYF1–GYF3) sediment profiles.

Organic carbon (OC) content showed pronounced vertical variability and clear differences among the six profiles (Figure 7). Elevated OC concentrations generally occurred in the uppermost layers, followed by a rapid decrease with depth, particularly in GYM1, GYF1, GYM2 and GYF3. The highest surface OC content was recorded in GYF3, reaching 7.14%. Below the surface zone, OC generally remained low, although several profiles exhibited secondary increases at greater depths. The most pronounced subsurface enrichment occurred in GYM3, where OC increased markedly below approximately 300 cm and remained high over a relatively thick interval, reaching a maximum of approximately 7.6%. A smaller but distinct increase was also observed in GYF2 at approximately 330–370 cm. Overall, OC showed stronger vertical differentiation than most of the other physicochemical parameters, with both surface enrichment and profile-specific deeper OC-rich horizons.

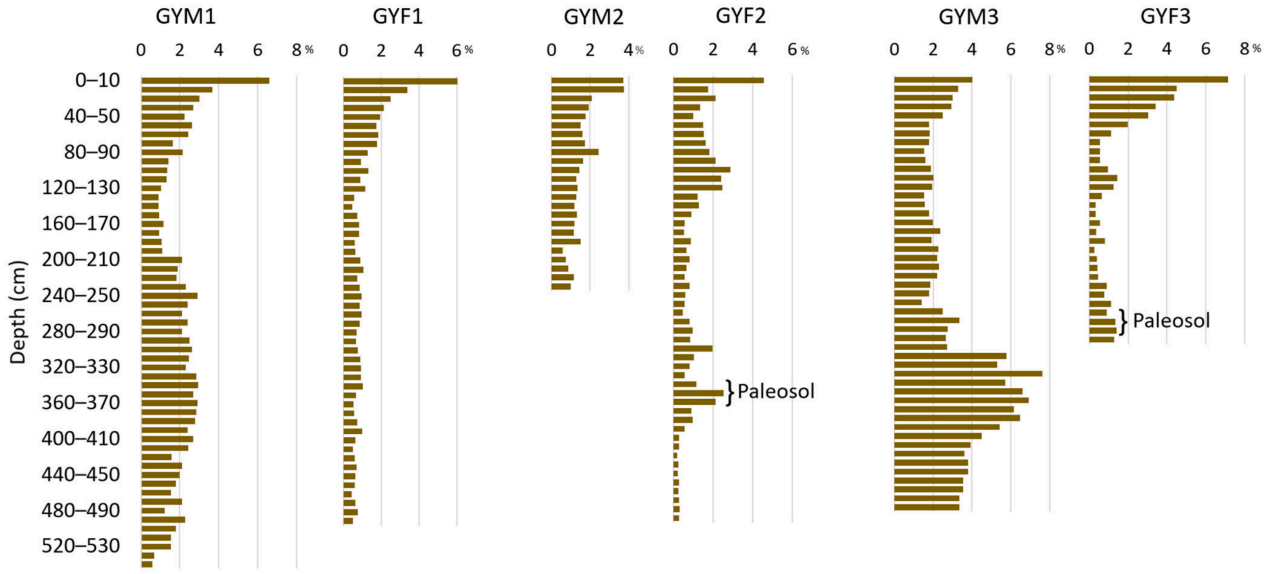


Figure 7. Vertical variation in organic carbon (OC) of the oxbows (GYM1–GYM3) and natural levees (GYF1–GYF3) sediment profiles.

3.2. Statistical Analysis

Based on the distributional analyses, the variables deviated from the normal distribution to varying degrees. The Shapiro–Wilk test indicated a significant deviation from normality for all investigated variables ($p < 0.05$); however, the magnitude of the deviations differed considerably based on the test statistics and Q–Q plots. The strongest deviation was observed for the coarse and medium-grained sand fraction (W = 0.157), whose distribution was characterized by a large number of zero values, whereas coarse silt showed the closest approximation to a normal distribution (W = 0.988; $p = 0.028$).

3.2.1. Results of Correlation Analysis

The Spearman rank correlation analysis revealed numerous significant relationships among the investigated physical and chemical parameters (Figure 8). The strongest positive correlation was observed between the two pH measurement methods ($\rho = 0.94$; $p < 0.01$). Marked relationships were also identified among the grain size fractions. The small-grained and fine-grained sand fractions were positively correlated ($\rho = 0.69$; $p < 0.01$), whereas fine-grained sand showed strong negative correlations with both fine silt and clay ($\rho = -0.80$; $p < 0.01$ in both cases). In contrast, fine silt and clay exhibited a positive correlation ($\rho = 0.59$; $p < 0.01$).

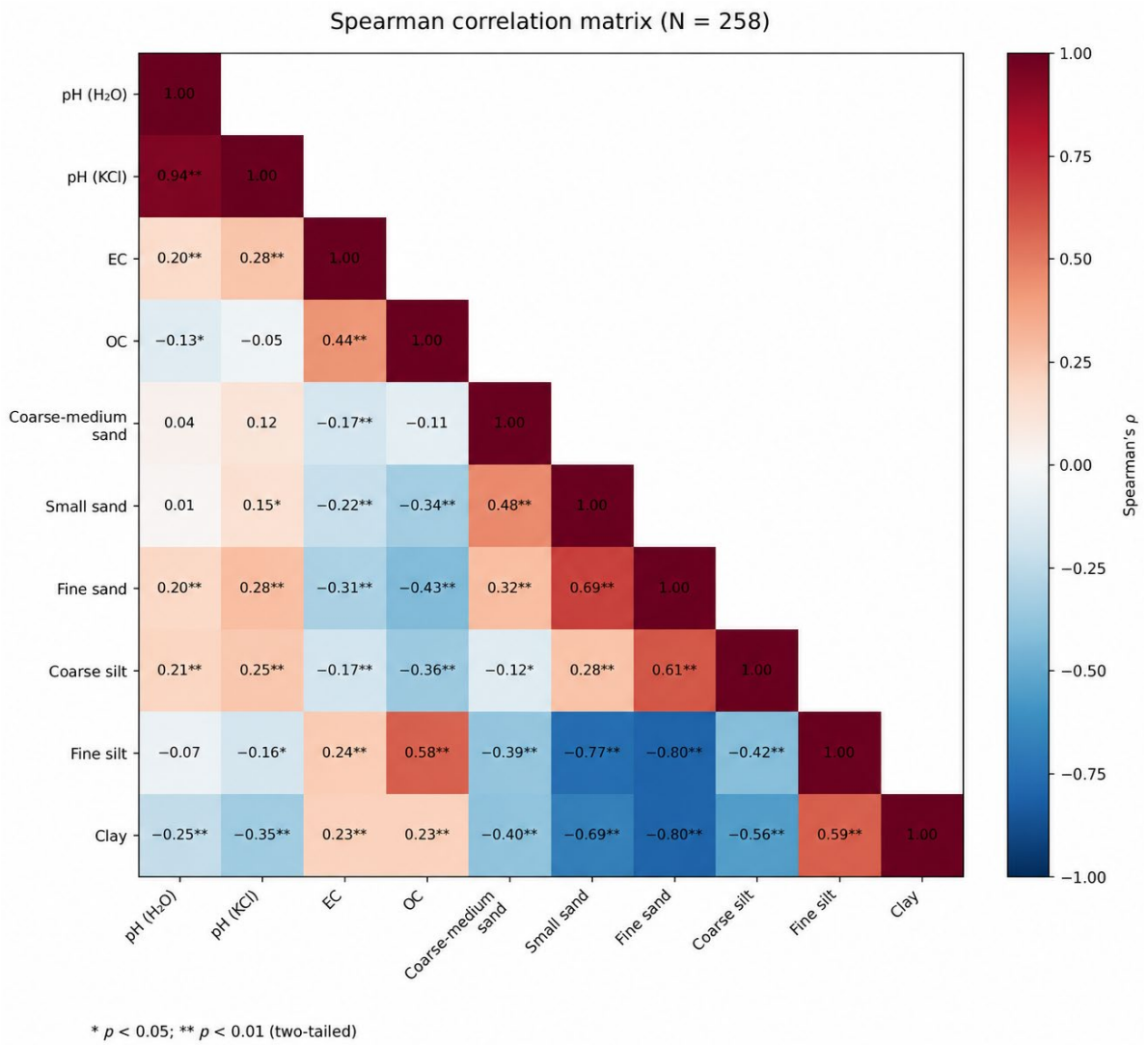


Figure 8. Spearman rank correlations among the investigated sedimentological and geochemical parameters (N = 258).

Several significant relationships were also observed between the geochemical parameters and grain size composition. OC was positively correlated with EC (ρ = 0.44; $p < 0.01$) and fine silt content (ρ = 0.58; $p < 0.01$), while showing negative relationships with fine-grained sand (ρ = −0.43; $p < 0.01$) and coarse silt (ρ = −0.36; $p < 0.01$). EC exhibited weak but significant positive correlations with fine silt and clay content (ρ = 0.24 and 0.23, respectively; $p < 0.01$), and was negatively correlated with fine-grained sand (ρ = −0.31; $p < 0.01$).

3.2.2. Principal Component Analysis

The assessment of the suitability of the data for principal component analysis yielded a Kaiser–Meyer–Olkin (KMO) value of 0.509, while Bartlett's test of sphericity was significant ($\chi^2 = 1526.868$; df = 28; $p < 0.001$). The relatively low KMO value indicates that the variables do not form a single strongly interrelated correlation structure. Based on the Kaiser criterion, four principal components with eigenvalues greater than 1 were retained. Together, the four retained components explained 88.53% of the total variance. After Varimax rotation, PC1 accounted for 29.63% of the variance, PC2 for 26.82%, PC3 for 16.94%, and PC4 for 15.14% (Table 3).

Table 3. Total Variance Explained.

Component	Initial Eigenvalues			Rotation Sums of Squared Loadings		
	Total	% of Variance	Cumulative %	Total	% of Variance	Cumulative %
1	3.216	40.205	40.205	2.371	29.633	29.633
2	1.501	18.766	58.971	2.146	26.821	56.454
3	1.232	15.401	74.372	1.355	16.940	73.394
4	1.133	14.159	88.531	1.211	15.137	88.531
5	0.580	7.253	95.783			
6	0.181	2.258	98.042			
7	0.130	1.630	99.671			
8	0.026	0.329	100.000			

Extraction Method: Principal Component Analysis.

The variables contributing to the individual principal components are presented in Table 4.

Table 4. Varimax-rotated component loadings of sediment properties.

	Component				Communality
	1	2	3	4	
pH(H_2O)	0.141	0.959	−0.120	−0.065	0.958
pH(KCl)	0.237	0.936	0.130	−0.005	0.949
EC	−0.101	0.210	0.851	0.064	0.782
OC	−0.118	−0.464	0.725	−0.126	0.771
ILR_1	0.780	0.202	−0.185	0.461	0.896
ILR_2	−0.076	−0.068	0.011	0.970	0.951
ILR_3	0.918	0.152	0.040	−0.131	0.885
ILR_4	0.902	0.149	−0.197	−0.129	0.890

PC1 was primarily determined by the high positive loadings of ILR_1 (0.780), ILR_3 (0.918), and ILR_4 (0.902), which represent grain size composition. Based on the combined direction of the three ILR coordinates, PC_1 represented a granulometric gradient from finer-grained sediments richer in clay and fine silt towards relatively coarser sediments with higher proportions of silt and sand (Table 5). The positive direction of PC1 therefore consistently indicated sediments with a relatively coarser grain size composition, meaning that high PC1 scores corresponded to relatively coarser sediments, whereas low PC1 scores indicated relatively finer sediments.

Table 5. Interpretation of the principal components.

PC	What Does it Represent?	Meaning of High Scores
PC1	General granulometric gradient	Relatively coarser-grained sediment
PC2	Acid–base gradient	Higher pH
PC3	OC–EC gradient	Higher OC and EC
PC4	Sand-fraction contrast	Higher proportion of small-grained sand relative to fine sand

PC2 was primarily determined by the high positive loadings of pH(H_2O) (0.959) and pH(KCl) (0.936). The component therefore represented an acid–base gradient. High PC2 scores indicated higher pH values, whereas lower PC2 scores reflected more acidic conditions (Table 5).

For PC3, EC (0.851) and OC (0.725) showed strong positive loadings. PC3 therefore represented geochemical variability related primarily to dissolved ions and organic matter content. High PC3 scores indicated simultaneously higher electrical conductivity and higher organic carbon content (Table 5).

PC4 was determined almost exclusively by the high positive loading of ILR_2 (0.970). Since ILR_2 expresses the relative ratio between the 0.2–0.1 mm and 0.1–0.05 mm sand fractions, the component represented the granulometric contrast between these two sand fractions. High PC4 scores indicated a relatively greater proportion of the 0.2–0.1 mm sand fraction, whereas low PC4 scores indicated a predominance of the 0.1–0.05 mm fine-grained sand fraction (Table 5).

The PCA results clearly demonstrate that the variability of the sediment samples collected from the investigated profiles is not organized along a single granulometric or geochemical gradient, but can be resolved into at least four clearly interpretable dimensions.

The rotated PC1 and PC2 components together explained 56.45% of the total variance, and the samples exhibited substantial variability along both components (Figure 9). In the PC1–PC2 score plot, samples from the individual profiles occupied partly distinct ranges, although considerable overlap was also observed. The separation of the samples was more pronounced along PC1, which represented the main grain-size gradient, whereas PC2, representing the acid–base gradient, provided additional differentiation.

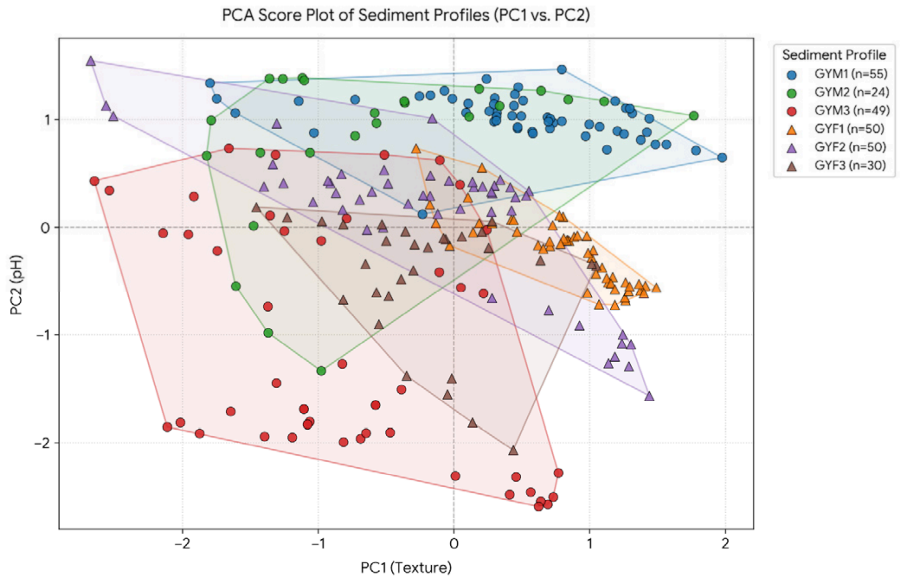


Figure 9. Distribution of samples from the investigated sediment profiles in the PC1–PC2 space.

The GYM3 samples extended across a wide range along PC1, covering both negative and positive score ranges and indicating substantial granulometric variability within the profile. In contrast, a considerable proportion of the GYM1 and GYF1 samples was located in the positive range of PC1, indicating a relatively coarser grain-size composition. Samples from the other profiles showed greater overlap in the PC1–PC2 space. Considerable within-profile dispersion was also observed along PC2, indicating that pH variability, which was partly independent of differences in grain-size composition, was also present within the individual profiles.

Overall, the PC1–PC2 distribution did not show complete separation either among the six profiles or between oxbow lake and natural levee samples. Instead, partially overlapping sample groups were formed, representing different combinations of granulometric and geochemical properties.

The PC1–PC3 score plot illustrates the joint variation in the granulometric and OC–EC gradients. The two rotated components together explained 46.57% of the total variance (Figure 10). Samples from the individual profiles also partially overlapped in this component space; however, several characteristic differences in their distributions were observed. The GYF1 samples formed a relatively compact group in the positive PC1 and negative PC3 ranges, whereas the GYM1 samples were likewise predominantly characterized by positive PC1 scores but exhibited substantially higher PC3 values, indicating higher organic matter content and electrical conductivity. This indicates that the relatively coarser granulometric character of samples from the two profiles was associated with different OC–EC properties.

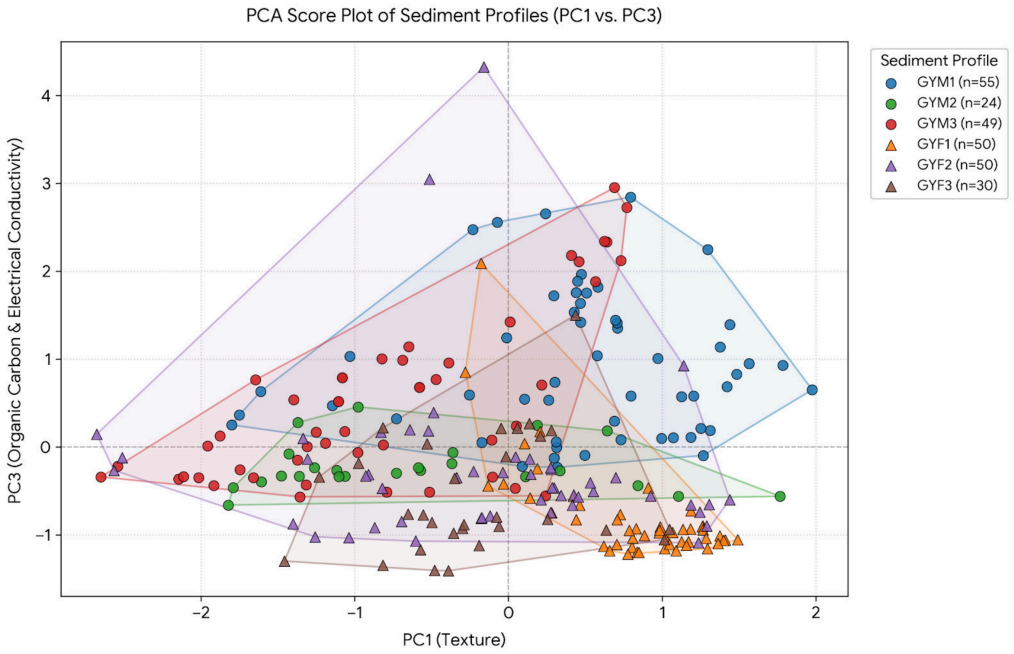


Figure 10. Distribution of samples from the investigated sediment profiles in the PC1–PC3 space.

In contrast, the GYM3 samples were distributed across a wide range of the PC1–PC3 space, indicating substantial granulometric and geochemical heterogeneity. Samples from GYM2, GYF2, and GYF3 showed greater overlap with one another. Overall, the PC1–PC3 distribution demonstrated that variability in grain size composition was not consistently associated with the OC–EC gradient; thus, similar granulometric characteristics may be associated with different geochemical properties.

The PC2–PC3 score plot showed more pronounced profile-specific structuring of the samples based on their geochemical properties than the previously examined component combinations (Figure 11). Together, the two rotated components explained 43.76% of the total variance.

The majority of the GYF1 samples formed a relatively compact group in both the negative PC2 and negative PC3 ranges. In contrast, the GYM1 samples were typically characterized by positive PC2 scores, with a substantial proportion also located in the positive PC3 range. Within GYM1, higher PC2 scores were in several cases associated with higher PC3 scores.

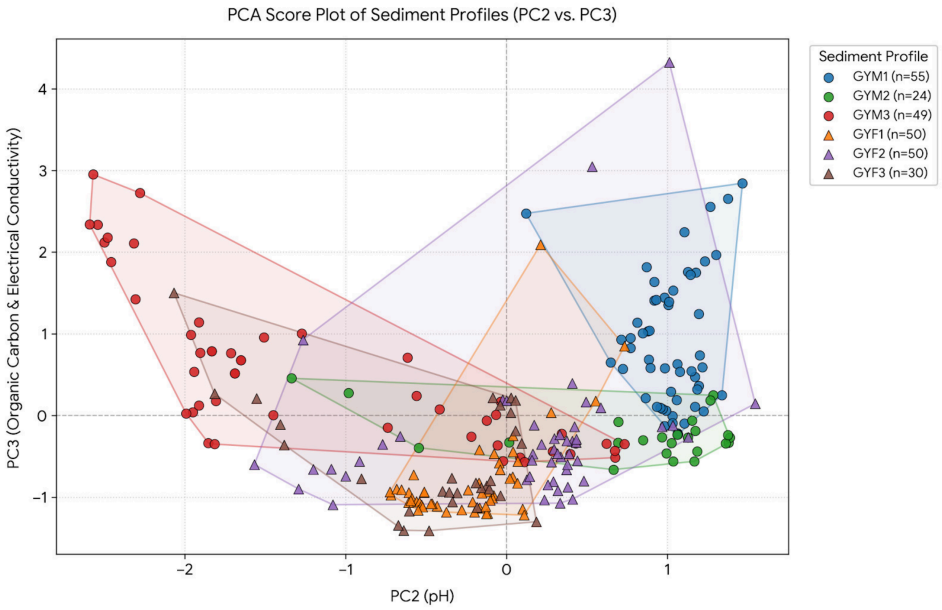


Figure 11. Distribution of samples from the investigated sediment profiles in the PC2–PC3 space.

GYM3 exhibited one of the greatest degrees of within-profile variability. Its samples covered a wide range of PC2 values, and a distinct sample group showed strongly negative PC2 scores combined with high positive PC3 values. In contrast, a substantial proportion of the GYF2 samples was concentrated in the negative PC3 range, while their PC2 values were higher than those of GYF1. The GYF3 and GYM2 samples showed greater overlap with samples from other profiles. Overall, the PC2–PC3 distribution indicated that the individual profiles were characterized by different combinations of acid–base and OC–EC properties, while substantial geochemical heterogeneity was also observed within some profiles.

3.2.3. Cluster Analysis

Hierarchical cluster analysis of the 258 sediment samples resulted in four main sample groups. The four-cluster solution was retained for interpretation because it provided a parsimonious and sedimentologically interpretable broad-scale grouping after exclusion of the $CaCO_3$-equivalent variable from the multivariate analysis. The resulting clusters contained 44 (C1), 112 (C2), 100 (C3), and 2 (C4) samples, respectively. The sensitivity analysis based on the four ILR coordinates together with pH(H_2O), EC, and OC retained the main structure of the primary classification, particularly for C1 and C2, although substantial redistribution occurred for C3 and the two-sample C4 did not remain a separate cluster.

The four clusters differed primarily in grain-size composition, pH, organic carbon content, and electrical conductivity. C1 represented a fine-grained, organic-rich group with comparatively low pH; C2 comprised predominantly fine-grained sediments with higher pH and lower organic carbon content; C3 was characterized by a substantially coarser grain-size composition and lower organic carbon content; while C4 consisted of only two exceptionally coarse basal samples (Table 6).

C1 was characterized by the highest organic carbon content (4.01%) and the lowest mean pH values among the four clusters (pH(H_2O) 5.02; pH(KCl) 4.05). Its grain-size composition was distinctly fine-grained, with fine silt and clay together accounting for approximately 78.9% of the sediment.

C2 also represented predominantly fine-grained sediments, but differed from C1 by its higher pH (pH(H_2O) 7.11; pH(KCl) 6.13) and lower mean organic carbon content (1.75%). Fine silt and clay together accounted for approximately 72.4% of the grain-size composition.

C3 was characterized by a substantially coarser grain-size composition. The combined mean proportion of the 0.2–0.1 mm and 0.1–0.05 mm sand fractions reached approximately 35.7%, while coarse silt accounted for a further 23.4%. The mean organic carbon content was relatively low (0.90%), and the mean pH(H_2O) was 6.77.

C4 contained only two samples and was clearly separated from the other clusters by its exceptionally coarse composition. Coarse- and medium-grained sand and the 0.2–0.1 mm sand fraction together accounted for approximately 81.0% of the sediment, whereas fine silt and clay together represented only about 7.7%.

Table 6. Physicochemical characteristics of the four clusters.

Variable	C1 (*n* = 44)	C2 (*n* = 112)	C3 (*n* = 100)	C4 (*n* = 2)	F
pH(H_2O)	5.02 ± 0.79	7.11 ± 0.52	6.77 ± 0.54	7.27 ± 0.03	141.56
pH(KCl)	4.05 ± 0.85	6.13 ± 0.87	5.71 ± 0.76	6.99 ± 0.01	70.34
EC (µS cm^{-1})	425 ± 187	418 ± 337	239 ± 183	453 ± 3	9.82
OC (%)	4.01 ± 1.65	1.75 ± 0.74	0.90 ± 0.51	0.64 ± 0.06	124.28
Coarse and medium-grained sand, 2–0.2 mm (%)	0.06 ± 0.25	0.05 ± 0.14	0.64 ± 1.62	33.50 ± 1.56	698.95
Small-grained sand, 0.2–0.1 mm (%)	3.25 ± 2.52	4.78 ± 3.38	16.89 ± 12.45	47.45 ± 2.05	62.89
Fine-grained sand, 0.1–0.05 mm (%)	4.45 ± 3.52	6.91 ± 4.47	18.83 ± 7.86	7.45 ± 0.07	94.73
Coarse silt, 0.05–0.02 mm (%)	13.38 ± 6.07	15.87 ± 7.58	23.44 ± 6.37	3.95 ± 0.35	33.81
Fine silt, 0.02–0.002 mm (%)	52.78 ± 4.62	46.82 ± 8.42	26.93 ± 7.89	5.70 ± 0.28	180.28
Clay, <0.002 mm (%)	26.08 ± 8.54	25.57 ± 11.78	13.27 ± 7.00	1.95 ± 0.50	36.73

Values are presented as mean ± standard deviation. F-values were obtained from one-way ANOVA. For all variables, $p < 0.001$. F-statistics are interpreted descriptively because the variables were also used to derive the clusters.

Descriptively, the largest F-value was obtained for coarse and medium-grained sand (F = 698.95), followed by fine silt (F = 180.28), pH(H_2O) (F = 141.56), and OC (F = 124.28). Fine-grained sand (F = 94.73), pH(KCl) (F = 70.34), small-grained sand (F = 62.89), clay (F = 36.73), and coarse silt (F = 33.81) also contributed to the differentiation among clusters, whereas EC showed a markedly lower F-value (F = 9.82). These F-statistics are used only to describe the relative contribution of the variables to the derived cluster structure and not as independent tests of cluster validity. The particularly high F-value for the coarse- and medium-grained sand fraction should be interpreted cautiously because C4 contains only two exceptionally coarse basal samples.

3.2.4. Vertical Distribution of the Clusters

Cluster membership showed pronounced vertical structuring within the investigated profiles (Figure 12). Although neither sampling depth nor profile identification was included among the input variables of the cluster analysis, samples belonging to the same cluster frequently formed continuous depth intervals. The vertical pattern, however, differed considerably among the individual profiles.

Among the natural levee profiles, GYF1 exhibited the simplest structure: the uppermost 0–10 cm belonged to C1, the 10–90 cm interval to C2, and the entire 90–500 cm lower section to C3. GYF2 showed a more heterogeneous pattern, with C1 occurring at 0–10 and 80–100 cm, C2 at 100–160, 170–220, and 280–370 cm, and C3 at 10–80, 160–170, 220–280, and 370–500 cm. GYF3 was similarly heterogeneous: C1 occurred at 0–50 cm, while C2 and C3 alternated below this depth, with C2 at 50–130, 170–180, and 230–270 cm, and C3 at 130–170, 180–230, and 270–300 cm.

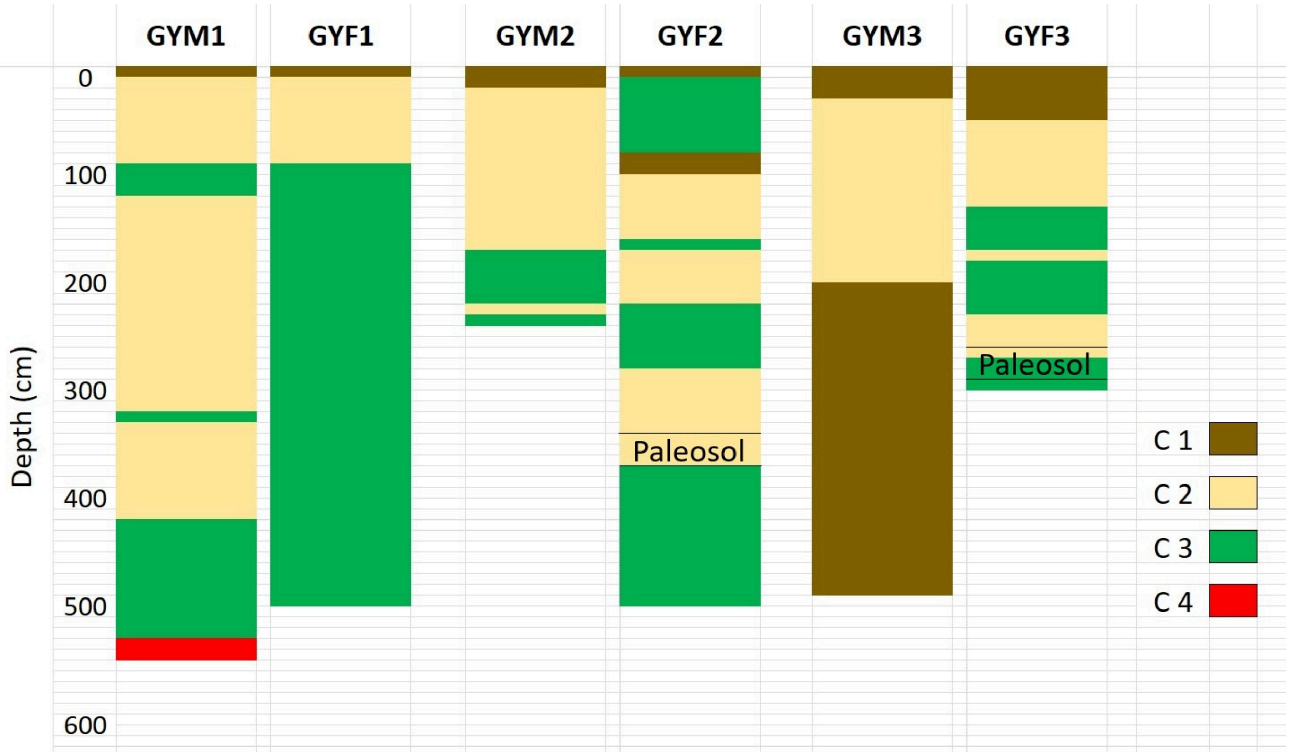


Figure 12. Vertical distribution of the four clusters across the six sediment profiles.

The oxbow lake profiles also exhibited distinct vertical patterns. In GYM1, C1 occurred only in the uppermost 0–10 cm, whereas C2 and C3 alternated throughout most of the profile. C2 occurred at 10–90, 120–320, and 330–420 cm, while C3 occurred at 90–120, 320–330, and 420–530 cm. The two deepest samples, at 530–550 cm, formed C4, which occurred exclusively in this profile. GYM2 was dominated by C2 between 20 and 180 cm, with C1 restricted to the uppermost 0–20 cm and C3 occurring mainly between 180 and 220 cm and again at 230–240 cm. The clearest zonation was observed in GYM3, where C1 occurred at 0–30 cm and continuously between 200 and 490 cm, while the intervening 30–200 cm section belonged entirely to C2.

4. Discussion

4.1. Correlation Analysis

The correlation structure reflects the interrelationships between the granulometric and geochemical properties of the investigated sediments. The strong negative relationships between the sand fractions and the finer silt–clay fractions, together with the positive correlation between fine silt and clay, indicate the differentiation of sediments deposited under different hydrodynamic conditions (Figure 8).

The higher OC values associated with finer-grained sediments, particularly the positive correlation between OC and fine silt and the negative correlation between OC and fine-grained sand, suggest that lower-energy depositional environments may have provided more favourable conditions for organic matter accumulation. The similar, although weaker, relationship between EC and the fine fractions likewise indicates an association between grain size composition and geochemical characteristics. Overall, these results support the interpretation that depositional environments with different energy levels alternated within the investigated sediment sequences, and that these variations are reflected not only in grain size composition but also in the geochemical properties of the sediments (Figure 8).

The relationship between fine-grained sediment and OC is also well supported by previous studies [2]. Sutfin & Wohl [50] demonstrated, based on 660 floodplain samples, that silt and clay content, sand content, and sample depth were significant predictors of OC, while Craft et al. [51] demonstrated long-term carbon sequestration associated with the deposition of fine sediments in floodplain wetlands in the Czech Republic and the United States. These findings are consistent with the positive OC–fine silt and negative OC–fine-grained sand relationships identified in the present study.

4.2. PCA

The substantial spatial overlap of the profiles in PCA space indicates that there is no simple, unambiguous correspondence between geomorphological form and the multivariate properties of the sediments (Figures 9–11). Similar granulometric and geochemical conditions may occur in profiles of different ages and geomorphological settings. This is consistent with the temporal variability of floodplain depositional environments, whereby different depths within the same profile may represent different depositional conditions, while individual layers from different profiles may record similar depositional conditions.

Given the continuous gradients identified by the PCA, discrete floodplain environments should therefore not be delineated solely on the basis of the PCA results; hierarchical cluster analysis is more suitable for identifying groups of samples with similar sedimentological and geochemical characteristics.

A similar methodological relationship was demonstrated by Oyedotun [52] in the Camel Estuary, where PCA revealed the principal axes of variation in grain size distribution, whereas the differentiation of samples according to sedimentary facies became more apparent when cluster analysis was applied, highlighting the complementary roles of the two multivariate methods in the interpretation of depositional environments.

The relatively distinct profile-specific separation observed in the PC2–PC3 component space indicates that differences among the sediment sequences are not determined exclusively by grain size composition (Figure 11). The individual profiles were also characterized by different combinations of acid–base conditions, as well as organic carbon and electrical conductivity. This is particularly important because it indicates that sediments with similar grain size compositions may have substantially different geochemical properties. The observed differences may therefore not solely reflect the hydrodynamic conditions prevailing during deposition, but may also record the influence of other characteristics of the depositional environment and processes operating after sediment deposition.

4.3. Environmental Interpretation of the Clusters

The four-cluster solution identifies broad sedimentological and geochemical states associated with different depositional and post-depositional conditions. The clusters frequently form vertically continuous intervals within the profiles (Figure 12); however, this vertical continuity should not be regarded as independent validation of the cluster solution because adjacent samples within sediment profiles are inherently spatially autocorrelated. Their environmental interpretation is therefore based primarily on differences in grain-size composition, pH, organic carbon content, and electrical conductivity, together with their stratigraphic distribution within the profiles. The possible influence of the change from profile-wall to auger sampling was also considered. In the four-cluster solution, a cluster boundary coincided exactly with the sampling-method transition in only two of the six profiles (GYF2 and GYM1), whereas no such coincidence occurred in GYF1, GYF3, GYM2, or GYM3. Thus, the overall vertical cluster pattern cannot be explained systematically by the change in sampling method, although a local methodological influence at the coincident boundaries cannot be completely excluded.

The C1 cluster represents fine-grained, organic-rich sediments characterized by the highest mean OC content and the lowest mean pH values among the four clusters (Table 6; Figure 12). The cluster occurs in two contrasting stratigraphic settings: in near-surface layers of several profiles and, most prominently, throughout the 200–490 cm interval of GYM3. This distribution indicates that C1 should not be interpreted as a single depositional environment, but rather as a recurring sedimentary–biogeochemical state characterized by fine texture, organic-matter enrichment, and relatively acidic conditions. In near-surface samples, these properties may reflect vegetation inputs and pedogenic modification. In contrast, the thick C1 interval in GYM3 is more consistent with prolonged water saturation and low-energy depositional conditions, which may have favoured organic-matter preservation [53,54]. Organic acids produced during decomposition and humification may also have contributed to the low pH of these sediments [55]. Field observations indicating increasingly reducing conditions at depth further suggest that reduced sulfur compounds may have formed; their subsequent oxidation during sample drying and exposure to oxygen could have contributed to sediment acidification [56,57]. Because sulfur species were not measured, however, this mechanism should be regarded as a plausible contributing process rather than a demonstrated cause.

The C2 cluster comprises predominantly fine-grained sediments characterized by relatively high pH and moderate organic carbon content (Table 6, Figure 12). Fine silt and clay together account for approximately 72% of the grain-size composition, while sand fractions remain comparatively low. The cluster occurs in several profiles over relatively thick intervals, indicating that it represents a common low-energy sedimentary state within the investigated floodplain sequences. Compared with C1, C2 lacks the pronounced organic-matter enrichment and acidity, suggesting weaker post-depositional acidification and less intense organic matter accumulation. Its widespread occurrence in both oxbow-lake and natural-levee profiles indicates that C2 should be interpreted as a broadly recurring fine-grained depositional state rather than as a sediment type restricted to a single geomorphological setting.

The C3 cluster is characterized by a substantially coarser grain-size composition than C1 and C2, with the combined proportion of the two sand fractions reaching approximately 36%, accompanied by a relatively high coarse-silt content (Table 6, Figure 12). Organic carbon content is comparatively low, indicating limited organic-matter accumulation. The cluster occurs mainly in deeper sections of several profiles, particularly in GYF1 and GYM1, where it forms relatively thick intervals. These characteristics are consistent with deposition under higher-energy fluvial conditions and stronger hydrological connectivity than those represented by C1 and C2. C3 may therefore be interpreted as a broadly recurring higher-energy fluvial sedimentary state, including channel-proximal overbank deposition and relatively energetic phases of oxbow-lake infilling.

The C4 cluster is clearly distinct from the other clusters and contains only two samples from the lowermost section of GYM1 at 530–550 cm depth. Its exceptionally coarse, sand-dominated composition is unique within the investigated sediment material (Table 6, Figure 12). The combined proportion of coarse- and medium-grained sand and the 0.2–0.1 mm sand fraction reaches approximately 81%, whereas the fine fractions are only weakly represented. Together with its basal stratigraphic position, these characteristics strongly suggest that C4 represents sediment deposited under active-channel conditions prior to cutoff. A comparable vertical transition from coarse basal channel deposits to progressively finer overlying sediments was described by Kiss et al. [58] from a paleochannel on the Bereg Plain.

4.4. Evolutionary Interpretation of the Oxbow Lake–Natural Levee Systems

Based on the vertical distribution of the clusters, the three oxbow lake–natural levee pairs exhibit different developmental and depositional trajectories. The metre-scale cluster intervals observed in several profiles, interpreted together with their stratigraphic position and sedimentological characteristics, provide an opportunity to reconstruct changes in depositional conditions through time.

In the youngest profile, GYM1, which was cut off in 1974, the basal C4 interval at 530–550 cm represents the exceptionally coarse sediment deposited under active-channel conditions prior to cutoff. Above this layer, the profile is dominated by alternating C2 and C3 intervals, indicating repeated shifts between relatively finer-grained, lower-energy sedimentation and coarser, higher-energy fluvial deposition (Figure 12). The alternation of these sedimentary states suggests that the reduction in depositional energy after cutoff was not monotonic and that periods of more quiescent infilling were interrupted by renewed higher-energy sediment input, most likely during flood events. The uppermost C1 layer reflects a more organic-rich and fine-grained sedimentary state that may indicate increasing surface stabilization and post-depositional modification. Overall, the vertical sequence records the transition from active-channel conditions towards progressive oxbow-lake aggradation, while retaining evidence of substantial variability in hydrological connectivity during infilling [18,20,59]. Using the 530 cm infill thickness above the former channel-bed sand, the 1974 cutoff date, and 2026 as the end year, the time-averaged post-cutoff sediment accumulation rate is estimated at approximately 10.2 cm yr^{-1}.

The associated GYF1 natural levee has a relatively simple vertical structure. The uppermost 0–10 cm belongs to C1, the 10–90 cm interval to C2, whereas the entire 90–500 cm lower section is assigned to C3 (Figure 12). This pattern indicates that most of the preserved profile consists of relatively coarse, higher-energy fluvial deposits, consistent with channel-proximal natural-levee accretion. The transition to C2 and finally to the thin surface C1 layer reflects a shift towards finer-grained sedimentation and increasing post-depositional modification near the surface. The uppermost C1 layer is also characterized by higher organic carbon content, consistent with vegetation input and pedogenic influence.

The GYM2 oxbow lake, which was cut off in 1852, exhibits a relatively simple vertical structure. The uppermost 0–20 cm belongs to C1, the 20–180 cm interval is dominated by C2, whereas C3 occurs between 180–220 cm and again at 230–240 cm, separated by a short C2 interval at 220–230 cm (Figure 12). This vertical pattern indicates a general upward transition from relatively coarser, higher-energy sedimentation towards finer-grained, lower-energy conditions, consistent with progressive hydrological isolation during oxbow-lake infilling. Compared with GYM1, the smaller number of transitions between C2 and C3 suggests a less variable depositional history within the analyzed part of the sequence. The channel sediment marking the base of the oxbow lake was reached at a depth of 780 cm using drilling equipment that did not allow sampling at 10 cm intervals. Based on the 780 cm depth of the former channel bed, the 1852 cutoff date, and 2023 as the end year, the whole-fill post-cutoff mean aggradation rate is estimated at 4.56 cm yr^{-1}. This value represents a time-averaged rate over the entire history of channel infilling and should not be interpreted as a constant sedimentation rate. Independent ^{137}Cs measurements from the upper part of the GYM2 profile provide evidence for substantially slower accumulation during the later stage of infilling. The bomb-fallout ^{137}Cs maximum occurs at 38–40 cm depth and yields an estimated mean accumulation rate of approximately 0.6 cm yr^{-1} for the period since the mid-1960s [36]. The marked difference between this recent rate and the whole-fill average indicates that sediment accumulation was considerably faster during the earlier stages following cutoff and subsequently slowed as the oxbow lake became progressively filled and hydrologically isolated. Based on the approximately

740 cm of sediment accumulated below the ^{137}Cs marker horizon, the mean accumulation rate during the earlier stage of infilling was approximately 6.6 cm yr^{-1}. This value should also be regarded as a time-averaged estimate, because sedimentation immediately after channel abandonment was probably substantially faster than this mean. Such strongly nonlinear infilling is consistent with observations from recently abandoned channels; Sedláček et al. [18], for example, reported initial sedimentation rates of up to approximately 32 cm yr^{-1} during the first 4–7 years after abandonment. The associated GYF2 natural levee exhibits a heterogeneous vertical structure, with repeated alternations between C2 and C3 below the near-surface section (Figure 12). The buried paleosol identified at 340–370 cm depth belongs entirely to C2 and is characterized in the field by its pitch-black colour, sharp boundaries, distinct thickness, and stratigraphic position. Similar buried soil horizons were widely observed in borrow-pit exposures across the Bereg Plain in 2015, several of which were subsequently investigated by Kiss et al. [58]. Their study demonstrated considerable lateral variability in paleosol preservation: up to three superimposed paleosol horizons occurred at some sites, whereas towards more distal parts of the alluvial ridges sedimentary layers thinned and paleosols merged, reducing the number of distinguishable horizons. Kiss et al. [58] obtained calibrated radiocarbon ages for five buried paleosol horizons on the Bereg Plain. Of particular relevance to the present study, two paleosols occurred at nearly identical depths on ridge F: T2carb at 290 cm, dated to 7460–7950 cal BP, and T3carb at 280 cm, dated to 3690–5492 cal BP. Because only a single prominent paleosol horizon was identified in GYF2 and its chronological equivalence with either of these dated horizons cannot be established, both age ranges were considered as plausible stratigraphic analogues. Using the upper boundary of the GYF2 paleosol at 340 cm depth and 2023 as the end year, the older age range yields a conditional long-term mean accretion rate of approximately 0.042–0.045 cm yr^{-1}, whereas the younger age range yields approximately 0.061–0.090 cm yr^{-1}. Accordingly, the plausible long-term mean accretion rate for GYF2 is approximately 0.042–0.090 cm yr^{-1}. This range should be regarded as a conditional estimate rather than a directly dated sedimentation rate. Nevertheless, it is broadly consistent with the accretion rate previously published for the upper part of the same profile, where the 16 cm thick layer formed after 1852 yielded an estimated rate of approximately 0.1 cm yr^{-1} [35]. The geomorphological positions of GYF1 and GYF2 differ considerably: GYF1 is located approximately 900 m from the Tisza River, whereas GYF2 lies about 1500 m from the river and is situated approximately 60 cm higher. These positional differences may have influenced their long-term sedimentary development, although no numerical accretion rate is assigned to GYF1 because of the absence of an independent chronological marker.

The vertical structure of the GYM3 oxbow lake shows a distinctive zonation, with C1 occurring between 200 and 490 cm, C2 between 30 and 200 cm, and C1 again in the uppermost 0–30 cm. The nearly 3 m thick lower C1 interval indicates that fine-grained, organic-rich and relatively acidic conditions persisted for an extended period during the development of the oxbow lake. As discussed above, this interval is consistent with prolonged water saturation, weak fluvial connectivity and enhanced preservation of organic matter. Its replacement by C2 above 200 cm indicates a shift towards a less organic-rich and less acidic fine-grained sedimentary state, while the reappearance of C1 in the uppermost 30 cm most likely reflects a different process, namely surface organic-matter accumulation and pedogenic modification. Thus, although the same cluster occurs in both the deep and surface parts of the profile, its environmental significance is not necessarily identical in the two stratigraphic settings. The channel sediment marking the base of the oxbow lake was reached at a depth of 1100 cm, again using drilling equipment that did not allow sampling at 10 cm intervals. Since the date of cutoff is unknown, it is only known that the channel was

already inactive at the time of the First Military Survey in 1785. Using the 1100 cm depth of the former channel bed, 1785 as the latest possible date of channel abandonment, and 2023 as the end year, the long-term mean aggradation rate can be estimated at a maximum of approximately 4.62 cm yr^{-1}. Because the channel may have become inactive considerably earlier, this value represents an upper-bound estimate and the actual long-term mean rate may have been lower.

The associated GYF3 natural levee exhibits an alternating C2–C3 structure below the upper C1 interval, with C2 occurring at 50–130, 170–180, and 230–270 cm, and C3 at 130–170, 180–230, and 270–300 cm (Figure 12). The buried paleosol horizon identified at 260–290 cm therefore spans the transition between C2 and C3. Its identification was based on the same characteristic field properties as in GYF2, including its pitch-black colour, sharp boundaries, distinct thickness, and stratigraphic position. Using the upper boundary of the GYF3 paleosol at 260 cm depth, 2023 as the end year, and the two alternative calibrated age ranges reported by Kiss et al. [58], the older age range yields a conditional long-term mean accretion rate of approximately 0.032–0.035 cm yr^{-1}, whereas the younger age range yields approximately 0.047–0.069 cm yr^{-1}. Accordingly, the plausible long-term mean accretion rate for GYF3 is approximately 0.032–0.069 cm yr^{-1}. As in GYF2, this range should be regarded as a conditional estimate rather than a directly dated sedimentation rate. The rates calculated from the Gyüre profiles should therefore be interpreted as long-term, profile-scale averages rather than constant sediment deposition rates, because oxbow aggradation is characteristically nonlinear and may include an initially rapid phase followed by progressively slower aggradation as hydrological connectivity decreases and the abandoned channel becomes stabilized. The lower accumulation rates reported in our previous study [35] were derived from the upper sediment sequences and therefore represent only part of the post-cutoff infill history. In GYM2, however, the earlier estimate refers to a time interval that substantially overlaps with the period considered here, indicating that the difference between the previously reported and whole-fill rates primarily reflects differences in the sampled sediment thickness and stratigraphic interval rather than simply different time spans. The two estimates should therefore be interpreted as complementary measures of sediment accumulation at different vertical scales within the same infill sequence. Considerable spatial and temporal variability in sediment accumulation has also been reported from the Upper Tisza floodplain. Szabó et al. [60] estimated accumulation rates of approximately 0.9–1.0 cm yr^{-1} in the Foltos-kert oxbow lake and 0.87 cm yr^{-1} in the nearby Boroszló-kert cut-off meander. The substantially higher whole-fill rate estimated for GYM2 may partly reflect differences in sampling position within the former channel. In GYM2, drilling was carried out close to the former thalweg, where the thickness of post-cutoff sediment accumulation is expected to be greatest. In contrast, the profiles reported by Szabó et al. [60] were not sampled at the deepest parts of the abandoned channels because standing water prevented coring at those locations. Consequently, the sediment thickness measured at those sites was lower, which would also result in lower calculated long-term mean accumulation rates. Molnár et al. [61], based primarily on repeated elevation measurements along floodplain cross-sections between 1976 and 2014, reported mean accumulation rates of 0.73–1.23 cm yr^{-1}, while substantially higher values of 4.44–8.13 cm yr^{-1} occurred at the lowest points of cut-off meanders and swales. The same study reported lower long-term mean rates of 0.84–2.5 cm yr^{-1} for three nearby cut-off meanders over periods of 154–161 years and interpreted the higher recent floodplain-wide values as evidence of accelerated accumulation associated with increasing surface roughness. Importantly, however, this comparison was based on different methods, time intervals, and geomorphological positions and did not document temporal acceleration within the same point of an individual cut-off channel. This distinction is

relevant to GYM2, where the whole-fill post-cutoff mean of 4.56 cm yr^{-1} contrasts with the approximately 0.6 cm yr^{-1} rate indicated by the upper-profile ^{137}Cs record since the mid-1960s. In this case, the two estimates refer to different stages of the same channel fill and therefore indicate a pronounced long-term slowdown in accumulation. Such a pattern is consistent with rapid early infilling after cutoff followed by progressively slower sedimentation as the channel becomes shallower and hydrologically more isolated.

4.5. Joint Interpretation of PCA and Cluster Analysis

PCA and cluster analysis provided complementary perspectives on the heterogeneity of the floodplain sediments. PCA identified the principal continuous gradients in sediment properties, whereas cluster analysis delineated discrete sediment groups with characteristic granulometric and geochemical properties (Figures 9–12). Together, the analyses indicate that sediment differentiation reflects not only grain-size and depositional-energy contrasts but also hydrological, geochemical, and pedogenetic processes. Their combined interpretation therefore provides a framework for reconstructing changes from active-channel conditions through oxbow aggradation to surface stabilization.

The main contribution of this combined approach is therefore not the identification of a simple correspondence between geomorphological units and sediment properties, but the recognition of recurring multivariate sediment states and vertically organized depositional zones across floodplain forms of different developmental stages.

4.6. Methodological Considerations and Limitations

Several methodological, spatial, and chronological constraints should be considered when interpreting the results of the present study. Each geomorphological unit is represented by a single sediment core, which restricts the number of spatially independent profiles and does not fully capture lateral variability within individual oxbow lakes and natural levees. Chronological constraints also differ among the investigated profiles. The abandonment ages of GYM1 and GYM2 are constrained by documented river-regulation events, whereas the exact abandonment age of GYM3 is unknown; historical cartographic evidence only demonstrates that the channel was already abandoned by 1785. The chronology of the natural-levee sequences partly relies on regional stratigraphic correlations and therefore carries greater uncertainty. Consequently, the calculated accumulation rates should be regarded as long-term, profile-scale estimates rather than temporally constant sedimentation rates. Independent geochronological measurements, including ^{137}Cs analyses, are currently in progress. Preliminary ^{137}Cs-based results are already available for the upper parts of selected profiles, whereas measurements of deeper sediment layers and additional profiles are still ongoing. The complete dataset will be presented separately and will provide an opportunity to further evaluate the sediment-accumulation patterns reconstructed in the present study.

A further limitation is the relatively low overall KMO value (0.509), indicating modest common variance among the variables and therefore requiring caution in interpreting the PCA structure. Nevertheless, all retained-variable communalities exceeded 0.77, and the four-component solution remained clearly interpretable after exclusion of the $CaCO_3$-equivalent variable from the PCA.

5. Conclusions

The investigated oxbow lake–natural levee systems revealed substantial differences in the vertical sedimentological and geochemical characteristics of the six profiles. Regarding RQ1, grain size composition, pH, electrical conductivity, $CaCO_3$-equivalent values, and organic carbon varied considerably both among and within profiles, reflecting differences

in depositional energy, hydrological connectivity, and post-depositional modification. The pronounced vertical heterogeneity indicates that the profiles preserve successive stages of floodplain development rather than uniform depositional environments.

In response to RQ2, multivariate analyses revealed a structured but complex organization of the sediments. PCA identified four major gradients related to grain size, acid–base conditions, OC–EC characteristics, and sand fraction composition, whereas cluster analysis distinguished four broad sediment groups with sedimentologically and geochemically interpretable characteristics. Thus, PCA and cluster analysis provided complementary information on continuous sedimentary gradients and discrete sedimentary states.

Regarding RQ3, the multivariate statistical analyses revealed vertical changes within the sedimentary sequences and helped identify sedimentological and geochemical differences associated with oxbow-lake infilling and natural-levee development. The considerable overlap among profiles in multivariate space demonstrates that geomorphological position alone does not determine sediment properties and that similar sedimentary states may occur in different landforms and at different depths. The stratigraphic succession of these states, interpreted together with the sedimentological observations, indicates changes in depositional energy, hydrological connectivity, organic matter accumulation, and post-depositional modification during floodplain development.

Regarding RQ4, long-term mean sediment accumulation rates were estimated independently of the multivariate analyses using sedimentological evidence together with available chronological and stratigraphic constraints. Time-averaged post-cutoff accumulation rates were approximately 10.2 cm yr^{-1} for GYM1 and 4.56 cm yr^{-1} for GYM2, while the $\leq$4.62 cm yr^{-1} estimate for GYM3 represents an upper-bound value because its exact cutoff date is unknown. No rate was estimated for GYF1 owing to the absence of an independent chronological marker. For GYF2 and GYF3, tentative correlation with alternative calibrated age ranges of dated paleosols reported from the Bereg Plain suggests conditional long-term mean accretion rates of approximately 0.042–0.090 and 0.032–0.069 cm yr^{-1}, respectively. These estimates indicate markedly different timescales of sediment accumulation in the investigated oxbow-lake and natural-levee sequences, while the indirect chronological constraints of the older profiles require cautious interpretation.

Overall, integrating vertical sedimentological and geochemical records with multivariate statistical analyses and independent chronological and stratigraphic constraints provides a framework for reconstructing relative depositional succession and estimating long-term sediment accumulation during floodplain evolution. This combined approach helps distinguish changes in depositional conditions from subsequent geochemical and pedogenic modification within oxbow lake–natural levee systems.

Author Contributions: Conceptualization, G.S. and R.V.; methodology, G.S. and R.V.; software, G.S., A.R., Z.T. and R.V.; formal analysis, G.S., A.R., G.N. and R.V.; investigation, G.S., A.R., P.C., D.B., T.M., D.N.M.O., Z.T., G.N. and R.V.; resources, G.S. and R.V.; data curation, G.S., A.R. and R.V.; writing—original draft preparation, G.S., A.R., P.C., D.B., T.M., D.N.M.O., Z.T., G.N. and R.V.; writing—review and editing, G.S., A.R., P.C., D.B., T.M., D.N.M.O., Z.T., G.N. and R.V.; visualization, G.S., A.R. and R.V.; supervision, G.S., A.R. and R.V. All authors have read and agreed to the published version of the manuscript.

Funding: Project no. TKP2021-NKTA-32 has been implemented with the support provided from the National Research, Development and Innovation Fund of Hungary, financed under the TKP2021-NKTA funding scheme.

Data Availability Statement: The data presented in this study are available on request from the corresponding author.

Conflicts of Interest: The authors declare no conflicts of interest.

References

1. Nanson, G.C.; Croke, J.C. A Genetic Classification of Floodplains. *Geomorphology* **1992**, *4*, 459–486. [CrossRef]
2. Wohl, E. An Integrative Conceptualization of Floodplain Storage. *Rev. Geophys.* **2021**, *59*, e2020RG000724. [CrossRef]
3. Van Appledorn, M.; Baker, M.E.; Miller, A.J. River-valley Morphology, Basin Size, and Flow-event Magnitude Interact to Produce Wide Variation in Flooding Dynamics. *Ecosphere* **2019**, *10*, e02546. [CrossRef]
4. Tofelde, S.; Bufe, A.; Turowski, J.M. Hillslope Sediment Supply Limits Alluvial Valley Width. *AGU Adv.* **2022**, *3*, e2021AV000641. [CrossRef]
5. Turowski, J.M.; Bufe, A.; Tofelde, S. A Physics-Based Model for Fluvial Valley Width. *Earth Surf. Dyn.* **2024**, *12*, 493–514. [CrossRef]
6. Ebel, U.; Engel, H. *The Christmas Floods in Germany 1993/1994*; Springer: München, Germany, 1994.
7. Hudson, P.F.; Middelkoop, H.; Stouthamer, E. Flood Management along the Lower Mississippi and Rhine Rivers (The Netherlands) and the Continuum of Geomorphic Adjustment. *Geomorphology* **2008**, *101*, 209–236. [CrossRef]
8. Hudson, P.F.; Sounny-Slitine, M.A.; LaFevor, M. A New Longitudinal Approach to Assess Hydrologic Connectivity: Embanked Floodplain Inundation along the Lower Mississippi River. *Hydrol. Process.* **2013**, *27*, 2187–2196. [CrossRef]
9. Scheel, K.; Morrison, R.R.; Annis, A.; Nardi, F. Understanding the Large-Scale Influence of Levees on Floodplain Connectivity Using a Hydrogeomorphic Approach. *JAWRA J. Am. Water Resour. Assoc.* **2019**, *55*, 413–429. [CrossRef]
10. Kiss, T. Fluviális Folyamatok Antropogén Hatásra Megváltozó Dinamikája: Egyensúly És Érzékenység Vizsgálata Folyóvízi Környezetben. Doctoral Dissertation, Hungarian Academy of Sciences, University of Szeged, Szeged, Hungary, 2014.
11. Cienciala, P.; Pasternack, G.B. Floodplain Inundation Response to Climate, Valley Form, and Flow Regulation on a Gravel-Bed River in a Mediterranean-Climate Region. *Geomorphology* **2017**, *282*, 1–17. [CrossRef]
12. Shukla, T.; Salas, C.R.; Pankau, R.C.; Rhoads, B.L. Critical Linkages among Floodplain Hydrology, Geomorphology and Ecology along a Lowland Meandering River, Illinois, USA. *Ecohydrology* **2024**, *17*, e2661. [CrossRef]
13. Asselman, N.E.M.; Middelkoop, H. Temporal Variability of Contemporary Floodplain Sedimentation in the Rhine–Meuse Delta, The Netherlands. *Earth Surf. Process. Landf.* **1998**, *23*, 595–609.
14. Middelkoop, H.; Asselman, N.E.M. Spatial Variability of Floodplain Sedimentation at the Event Scale in the Rhine–Meuse Delta, The Netherlands. *Earth Surf. Process. Landf.* **1998**, *23*, 561–573.
15. Walling, D.E.; Owens, P.N.; Leeks, G.J.L. The Characteristics of Overbank Deposits Associated with a Major Flood Event in the Catchment of the River Ouse, Yorkshire, UK. *CATENA* **1997**, *31*, 53–75. [CrossRef]
16. Klasz, G.; Reckendorfer, W.; Gabriel, H.; Baumgartner, C.; Schmalfuss, R.; Gutknecht, D. Natural Levee Formation along a Large and Regulated River: The Danube in the National Park Donau-Auen, Austria. *Geomorphology* **2014**, *215*, 20–33. [CrossRef]
17. Piégay, H.; Hupp, C.R.; Citterio, A.; Dufour, S.; Moulin, B.; Walling, D.E. Spatial and Temporal Variability in Sedimentation Rates Associated with Cutoff Channel Infill Deposits: Ain River, France. *Water Resour. Res.* **2008**, *44*, 2006WR005260. [CrossRef]
18. Sedláček, J.; Kapustová, V.; Šimíček, D.; Bábek, O.; Sekanina, M. Initial Stages and Evolution of Recently Abandoned Meanders Revealed by Multi-Proxy Methods in the Odra River (Czech Republic). *Geomorphology* **2019**, *333*, 16–29. [CrossRef]
19. Kiss, T.; Oroszi, V.G.; Sipos, G.; Fiala, K.; Benyhe, B. Accelerated Overbank Accumulation after Nineteenth Century River Regulation Works: A Case Study on the Maros River, Hungary. *Geomorphology* **2011**, *135*, 191–202. [CrossRef]
20. Toonen, W.H.J.; Kleinhans, M.G.; Cohen, K.M. Sedimentary Architecture of Abandoned Channel Fills. *Earth Surf. Process. Landf.* **2012**, *37*, 459–472. [CrossRef]
21. Constantine, J.A.; Dunne, T. Meander Cutoff and the Controls on the Production of Oxbow Lakes. *Geology* **2008**, *36*, 23. [CrossRef]
22. Sparks, D.L. *Environmental Soil Chemistry*, 2nd ed.; Elsevier: Amsterdam, The Netherlands, 2003.
23. Havlíková, P.; Chalupová, D.; Chuman, T.; Šobr, M.; Janský, B. Long-Term Water and Sediment Quality of the Elbe River's Oxbow Lake near the Town of Poděbrady, the Czech Republic. *Environ. Earth Sci.* **2019**, *78*, 559. [CrossRef]
24. Zheng, W.; Yang, Z.; Wang, X.; Wang, H.; Yu, X.; Wang, L.-P.; He, B. Impacts of Evaporation and Inundation on Near-Surface Salinity at a Coastal Wetland Park. *Mar. Pollut. Bull.* **2022**, *185*, 114373. [CrossRef]
25. Scott, D.N.; Wohl, E.E. Geomorphic Regulation of Floodplain Soil Organic Carbon Concentration in Watersheds of the Rocky and Cascade Mountains, USA. *Earth Surf. Dyn.* **2018**, *6*, 1101–1114. [CrossRef]
26. Fulajtár, E.; Mabit, L.; Renschler, C.S.; Yi, A.L.Z. *Use of ^{137}Cs for Soil Erosion Assessment*; Food and Agriculture Organization of the United Nations, International Atomic Energy Agency: Rome, Italy, 2017.
27. Mabit, L.; Benmansour, M.; Walling, D.E. Comparative Advantages and Limitations of the Fallout Radionuclides 137Cs, 210Pbex and 7Be for Assessing Soil Erosion and Sedimentation. *J. Environ. Radioact.* **2008**, *99*, 1799–1807. [CrossRef]
28. Kiss, K.T.; Acs, E.; Barkacs, K.; Borics, G.; Böddi, B.; Ector, L.; Solymos, G.K.; Szabo, K.; Varga, A.; Varga, I. Qualitative Short-Term Effects of Cyanide and Heavy Metal Pollution on Phytoplankton and Periphyton in the Rivers Tisza and Szamos (Hungary). *River Syst.* **2002**, *13*, 47–72. [CrossRef]

29. Nguyen, H.L.; Braun, M.; Szaloki, I.; Baeyens, W.; Van Grieken, R.; Leermakers, M. Tracing the Metal Pollution History of the Tisza River Through the Analysis of a Sediment Depth Profile. *Water. Air. Soil Pollut.* **2009**, *200*, 119–132. [CrossRef]
30. Brown, A.G.; Carpenter, R.G.; Walling, D.E. Monitoring Fluvial Pollen Transport, Its Relationship to Catchment Vegetation and Implications for Palaeoenvironmental Studies. *Rev. Palaeobot. Palynol.* **2007**, *147*, 60–76. [CrossRef]
31. Saint-Laurent, D.; St-Laurent, J.; Lavoie, L.; Ghaleb, B. Use Geopedological Methods for the Evaluation of Sedimentation Rates on River Floodplains, Southern Québec, Canada. *CATENA* **2008**, *73*, 321–337. [CrossRef]
32. Wallinga, J. Optically Stimulated Luminescence Dating of Fluvial Deposits: A Review. *Boreas* **2002**, *31*, 303–322. [CrossRef]
33. Rhodes, E.J. Optically Stimulated Luminescence Dating of Sediments over the Past 200,000 Years. *Annu. Rev. Earth Planet. Sci.* **2011**, *39*, 461–488. [CrossRef]
34. Kertész, T.G.; Hubay, K.; Buró, B.; Jull, A.J.T.; Mindszenty, A.; Sipos, G.; Bartyik, T.; Molnár, M. The Last 40,000 Years of a Floodplain Area (Tisza, Hungary) Comparative Case Study of ^{14} C and OSL Methods. *Radiocarbon* **2025**, *67*, 656–678. [CrossRef]
35. Vass, R.; Rooien, A.; Czomba, P.; Balázs, D.; Babka, B.; Szabó, G. Active Floodplain Sedimentation Dynamics in the Upper Tisza Region, Hungary, After River Regulation. *Land* **2026**, *15*, 322. [CrossRef]
36. Rooien, A.; Szabó, G.; Vass, R. Comparative Analysis of Sedimentation Rates in Meanders and Natural Levees of the Tisza River Floodplain (Bereg Plain, Hungary) Utilizing Cesium-137 (^{137}Cs) as a Tracer. In Proceedings of the EGU General Assembly 2026, Vienna, Austria, 3–8 May 2026.
37. Bogárdi, J. *Vízfolyások Hordalékszállítása*; Akadémiai Kiadó: Budapest, Hungary, 1971.
38. Lászlóffy, W. *A Tisza*; Akadémiai Kiadó: Budapest, Hungary, 1982.
39. Országos Vízügyi Főigazgatóság Országos Vízügyi Főigazgatóság. Available online: https://www.vizugy.hu/ (accessed on 30 August 2026).
40. Konecsny, K. A Felső-Tisza 1998-2001. évi árvizeinek hidrológiai értékelése. *Hidrol. Közlöny* **2003**, *83*, 75–85.
41. Csoma, J. *Árvízvédelem, Folyó-És Tószabályozás, Víziutak Magyarországon*; OVH: Budapest, Hungary, 1978.
42. Vass, R. *Ártérfejlődési Vizsgálatok Felső-tiszai Mintaterületeken*; Vass Róbert: Nyíregyháza, Hungary, 2018.
43. *MSZ 08-0205:1978*; A Talaj Fizikai és Vízgazdálkodási Tulajdonságainak Vizsgálata. Magyar Szabványügyi Testület: Budapest, Hungary, 1978.
44. Miháltz, I. Homokszemnagyság helyszíni meghatározása. *Földt. Közlöny* **1952**, *82*, 51–57.
45. *MSZ 08-0206-2*; A Talaj Egyes Kémiai Tulajdonságainak Vizsgálata. Laboratóriumi Vizsgálatok (pH-Érték, Szódában Kifejezett Fenolftalein Lúgosság, Vízben Oldható Összes só, Hidrolitos /y1-Érték/És Kicserélődési Aciditás/y2-Érték/). Magyar Szabványügyi Testület: Budapest, Hungary, 1978.
46. *MSZ-08-0210-1977*; Talajok Szerves Széntartalmának Elemzése. Magyar Szabványügyi Testület: Budapest, Hungary, 1977.
47. *MSZ 21470–2:1981*; Környezetvédelmi Talajvizsgálatok. Talajminta Előkészítése, Nedvességtartalom, Elektromos Vezetőképesség és pH Meghatározása. Magyar Szabványügyi Testület: Budapest, Hungary, 1981.
48. *IBM SPSS Statistics for Windows*, Version 22.0; IBM Corp.: Armonk, NY, USA, 2013.
49. Egozcue, J.J.; Pawlowsky-Glahn, V.; Mateu-Figueras, G.; Barceló-Vidal, C. Isometric Logratio Transformations for Compositional Data Analysis. *Math. Geol.* **2003**, *35*, 279–300. [CrossRef]
50. Sutfin, N.A.; Wohl, E. Substantial Soil Organic Carbon Retention along Floodplains of Mountain Streams. *J. Geophys. Res. Earth Surf.* **2017**, *122*, 1325–1338. [CrossRef]
51. Craft, C.; Vymazal, J.; Kröpfelová, L. Carbon Sequestration and Nutrient Accumulation in Floodplain and Depressional Wetlands. *Ecol. Eng.* **2018**, *114*, 137–145. [CrossRef]
52. Oyedotun, T.D.T. Compositional and Multivariate Statistical Analyses for Grain-Size Characterisation of Intertidal Sedimentary Facies in an Estuarine Environment. *Geol. Ecol. Landsc.* **2022**, *6*, 224–230. [CrossRef]
53. Sahrawat, K.L. Organic Matter Accumulation in Submerged Soils. In *Advances in Agronomy*; Elsevier: Amsterdam, The Netherlands, 2003; Volume 81, pp. 169–201.
54. Cunha-Santino, M.B.D.; Bianchini Júnior, I. Reviewing the Organic Matter Processing by Wetlands. *Acta Limnol. Bras.* **2023**, *35*, e19. [CrossRef]
55. Shotyk, W. Review of the Inorganic Geochemistry of Peats and Peatland Waters. *Earth-Sci. Rev.* **1988**, *25*, 95–176. [CrossRef]
56. Kawahigashi, M.; Do, N.M.; Nguyen, V.B.; Sumida, H. Effects of Drying on the Release of Solutes from Acid Sulfate Soils Distributed in the Mekong Delta, Vietnam. *Soil Sci. Plant Nutr.* **2008**, *54*, 495–506. [CrossRef]
57. Sullivan, L.A.; Ward, N.J.; Bush, R.T.; Burton, E.D. Improved Identification of Sulfidic Soil Materials by a Modified Incubation Method. *Geoderma* **2009**, *149*, 33–38. [CrossRef]
58. Kiss, T.; Sipos, G.; Vass, R. Alluvial Ridge Development and Structure: Case Study on the Upper Tisza, Hungary. *Geogr. Pannonica* **2022**, *26*, 230–240. [CrossRef]
59. Ishii, Y.; Hori, K. Formation and Infilling of Oxbow Lakes in the Ishikari Lowland, Northern Japan. *Quat. Int.* **2016**, *397*, 136–146. [CrossRef]

60. Szabó, J.; Tóth, C.; Vass, R. Examination of Fluvial Development on Study Areas of Upper-Tisza Region. *Carpathian J. Earth Environ. Sci.* **2012**, *7*, 241–253.
61. Molnár, G.; Scholtz, A.; Vass, R. Accumulation Studies at Specific Sampling Areas of the Active Floodplain in the Upper-Tisza Region. *ACTA Geogr. Debrecina Landsc. Environ.* **2017**, *11*, 14–22. [CrossRef]

Disclaimer/Publisher's Note: The statements, opinions and data contained in all publications are solely those of the individual author(s) and contributor(s) and not of MDPI and/or the editor(s). MDPI and/or the editor(s) disclaim responsibility for any injury to people or property resulting from any ideas, methods, instructions or products referred to in the content.